Memoirs of the Faculty of Engineering, Nagoya University
Vol. 40, No. 1 (1988)

DEVELOPMENT OF MEASURING AND CHARACTERIZING METHODS OF MECHANICAL PROPERTIES OF POWDER PARTICLES

GENJI JIMBO, RYOHEI YAMAZAKI*,
JUN-ICHIRO TSUBAKI** and HIDEHIRO KAMIYA***

Department of Chemical Engineering

(Received May 31, 1988)

Abstract

To make clear the fundamental characteristics of powder material and its behaviors, which are still very difficult to analyse and to predict quantitatively, several kinds of measuring principles and methods have been developed by the authors. And it was found that the results obtained by different methods scattered largely and showed very poor coincidence. Reasons for such big difference in the results of the measurement of adhesive properties are discussed analytically in this report. In the case of single particle measurement, the effects of the direction of separation force and the contact relation of particles are pointed out and new equations including these effects are proposed. In the case of podwer bed, the effect of compression force at the contact point is pointed out as one of the most essential factors which determine the strength of powder bed. Then based on the experimental finding about the relation between the tensile strength and the porosity of powder bed, modified Rumpf's equation is derived semi-theoretically and proposed here taking into account of the effect of compression force. Other measurement methods and their results of adhesive properties, such as deagglomeration of agglomerated powder assemblage in air stream and the change of adhesion force against temperature, are also shown. The latter are applied to the analysis of fluidized bed for predicting the incipient fluidization velocity at elevated temperature. Finally

* Department of Chemical Engineering, University of Tokyo
** Japan Fine Ceramics Center
*** Department of Inorganic Materials, Nagoya Institute of Technology

time-dependent properties, such as fatigue and creep, are proposed as new characterizing principles of powder materials. With all these results obtained experimentally and theoretically, the main causes of big difference of measured results of adhesion force by different methods are explained qualitatively.

Contents

1. Introduction

In many chemical and other engineering processes, the processes of treating powder materials are recognized as main cause of troubles. The blockage of hopper discharge is the most popular example, in which main difficulties lay on the fact that this kind of phenomenon is almost always non-reproducible.

And it is now extensively cleared that this sort of phenomenon is based on the mutual interaction of particles touched each other, and the most fundamental interactive force is adhesion or cohesion force of powder particles.

This force also plays a very important role in many unit operations related to powder materials, for example, granulation and dust collection. Therefore to characterize powder materials according to their mechanical properties, including adhesiveness, is very essential to predict their behavior in engineering processes. Indeed this characterization can also be applied to the prediction and understanding of many phenomena in natural circumstances.

But it has also been cleared that the methods to characterize mechanical powder properties have a wide variety of principles and types causing big scatter of measured results.

In this paper the authors intend to find the main reasons for such big scattering of data obtained, and to make clear some controlling factors of them for establishing more reliable measuring and characterizing methods of powder materials.

2. The development of the measuring methods of mechanical powder properties

2. 1. Measuring methods of single particle

When analytical investigation of the measuring methods of mechanical powder properties started systematically in 1950s, there were already various kinds of characterizing methods of powder properties, such as methods of angle of repose, packing density and flowability, which are shown in the right column of Table 2. 1. But they were all empirical and not analytical methods and therefore the results by them were able to be

Table 2. 1. Classification of measurement methods of mechanical powder properties

	Primary	Secondly	Multiple	
	Single Particle Measurement	Powder Bed Measurement	Practical Testing Type	
Simple	Spring balance Centrifugal separation Vibration separation Impaction (Inertia) separation	Tensile strength Horizontal type No Bearing type Suspension type Vertical type		
Complicated		Shear strength Linear shear box Ring shear box Bi-axial shear type Tri-axial shear type Dispersion in air flow	Fluidized bed Packing density Flowability	Angle of repose Hopper discharge Dispersability Dustability
Combined	Yield locus, Flow factor, Carr's flowability			

applied to relatively limited range, though they are still widely used in industry effectively.

In another side, there were some trials to measure the interaction force between solid surfaces to prove the physical theory proposed by London, Hamaker and Lifsitz, using the principles of spring balance and pendulum method, which are shown in the top left part of Table 2. 1. These methods are applicable only for pure scientific experiment, and not for engineering purposes, because for the latter it is essential to obtain reasonably enough number of data which can be treated statistically. This is because the characteristics of particles are always statistically distributed in wide range. The size of particle in powder materials is the best example.

Therefore to measure the adhesion force of reasonably large number of particles, centrifugal separation method had to be introduced. Jordan,[1] Larsen,[2] Kordecki,[3] Krupp and Zimon were the pioneers in the development of this method. Especially two of the latters wrote very influential review papers[4] and a book,[5] which afterward made it a sort of standard method.

2. 2. *Measuring methods of powder bed*

Powder materials behave, in many cases, as a mass, such as powder packed bed, contact bed in flowing state, fluidized bed and aggregated assemblage. All practical measuring methods, of which some examples are shown in the right end of Table 2. 1, are not based on the behavior of single particle, but of powder mass. Therefore it was necessary to bridge the gap between the single particle measurement methods and the practical methods indicated above by introducing some analytical measuring methods of powder bed.

Ashton, Farley and Valentine developed split cell type tensile strength measurement method nearly twenty five years ago,[6] and that principle is now widely accepted as a standard method, though there are many versions of the same principle, as will be shown in the following chapters.

Preceding to these methods, shear tester of soil bed had been developed in civil engineering field, and it was modified to apply to powder technology by Jenike.[7] This is another fundamental measurement method of characterizing mechanical powder property, but in this paper this method will be discussed only in very limited range.

3. Summarized results of the measurements of adhesive properties with standard methods

At the first stage of this research project, the authors measured the adhesion forces of both single particle and powder bed by using centrifugal separation method based on Krupp's idea,[4] and split-cell type tensile tester based on Ashton and his co-workers' idea.[6] Main points of our findings from the results can be summarized as follows.

(1) The distribution of the adhesion force of powder particle, which was found to be able to be represented by log-normal distribution, is very wide.[8] Therefore fifty percent average value of adhesion force, F_{50}, which shows the point where a half of particles adhere to a solid surface is detached, can not always show the representative value of powder properties related to adhesive behavior.

(2) The humidity of atmosphere is indeed very influencial, but the order of that effect on single particle adhesion force is not more than one order in the case of ordinary mineral materials.

(3) The effect of the shape of a particle is very large, sometimes larger than one order. A particle with smooth spherical surface shows more adhesive property than that with irregular shape by single particle measurement method.[8]

(4) The adhesion force of powder bed increases with the decrease of the porosity of the bed. And the relation between the tensile strength and the porosity of powder bed was found not to be represented by following Rumpf's equation.

$$\sigma_z = \frac{(1-\varepsilon)}{\varepsilon} \frac{F}{{d_p}^2} \tag{3.1}$$

And the formation and compaction method of powder bed affects to the final results. For instance, powder bed by compaction method has higher strength than that with the same porosity by tapping method.[9]

(5) The adhesion force by different methods were compared each other by converting the value of tensile strength of powder bed into the adhesion force of a single particle using Eq. (3.1) and other related equations.[10] For instance in fluidized bed method, the following equation was used to obtain the single particle adhesion force, F, from the incipient fluidization velocity, u_{mf}, in which the second term of the equation represents the effect of adhesion force, which prevents the hydrodynamical formation of air bubble in powder bed.[11]

$$u_{mf} = \frac{(\rho_s - \rho_f) g}{18 \beta \mu_f} {d_p}^2 + \frac{\alpha F}{3 \pi \beta \mu_f d_p} \tag{3.2}$$

where F is adhesion force at contact point, α is angle relation of contact and β indicates the effect of packing structure of the bed.

Simplified presentation of the results of such comparison is shown symbolically in Fig. 3.1. From this we can say that the most influential factor to determine the adhesion force of particles thus obtained is not material itself, but the methods used. The difference between the largest and smallest is the order of 10^7 or even more. Indeed here it must be pointed out that the conversion methods used include many uncertain assumptions, but even when such uncertain factors are taken into account, still the difference found here is much larger than first expected.

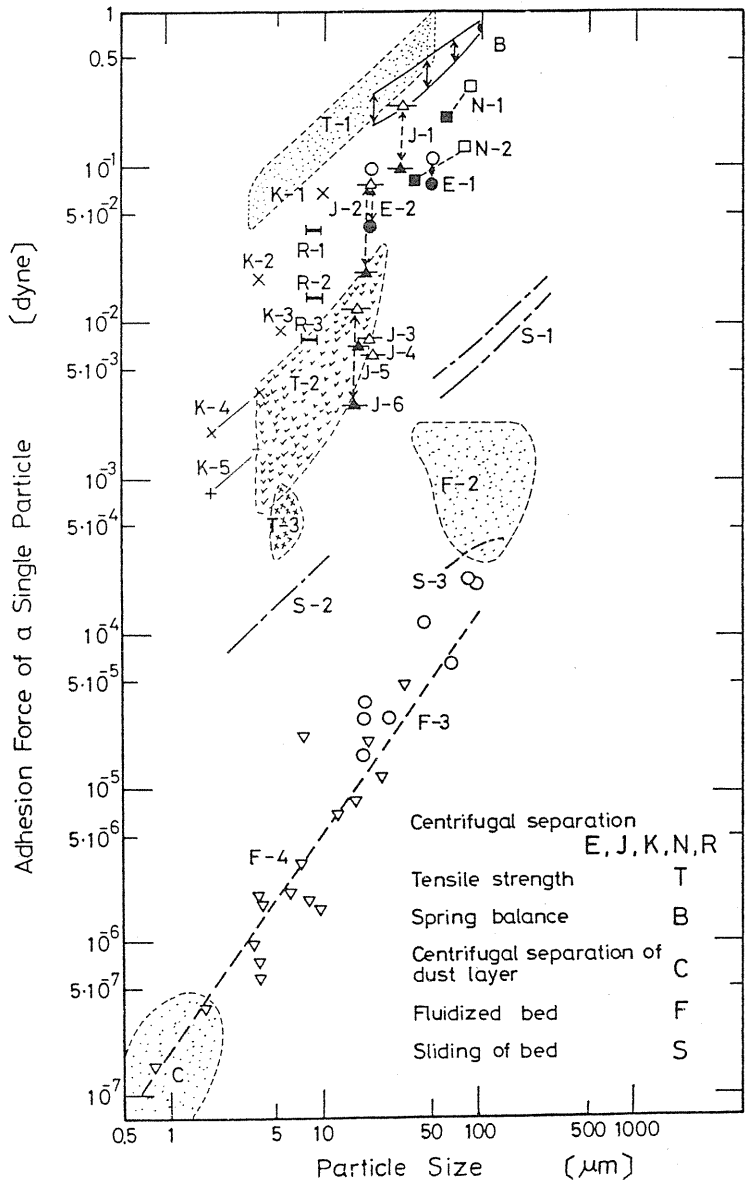

Fig. 3. 1. Measured results of adhesion force of single particle by different measuring principles and methods.

From the results of preliminary measurements described above, the problems to be solved to find some reasonable measuring methods of mechanical powder properties were found to be as follows.

(1) To find out the factors which made the adhesion force measured so widely distributed.

(2) In such factors, the effect of particle shape would be one of the most important.

(3) The conditions to form powder bed were another very important factor to determine not only the strength of powder bed but also the adhesion force of individual particles which constitute the powder bed. In another word, it would be necessary to obtain new or modified Rumpf's equation which expressed the relationship between the tensile strength of powder bed and the adhesion force of single particle.

In the following chapters, the problems deduced from the preliminary experiments about the measurement of mechanical powder properties summarized above will be examined and discussed, and some new findings will be shown. The proposals to describe some of the mechanical powder properties will be made.

4. The factors which affect the adhesion force of single particle

4. 1. Measurement of adhesion force by the principles other than centrifugal separation

Although the centrifugal separation method developed at the earliest stage of this research project was well-known and widely used as a standardized method, it was disadvantageous as a general routine method because of the complexity of the procedure and of the cost of equipment including centrifuge. Besides, it is not suitable for the measurement at high temperature. That condition is very essential for chemical engineering processes.

Accordingly other two principles, namely vibration separation (Fig. 4. 1) and impaction (inertia) separation (Fig. 4. 2) methods, were introduced and developed. Especially

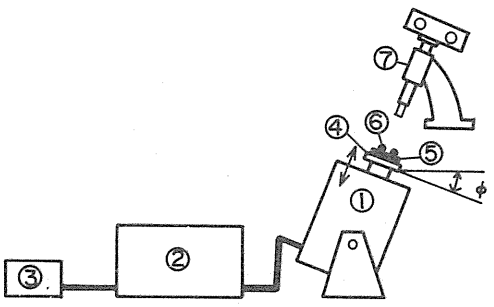

Fig. 4. 1. The experimental apparatus of vibration separation method. (① Vibrator ② Amplifier ③ Oscillator ④ Base ⑤ Plate ⑥ Particle ⑦ Microscope with camera).

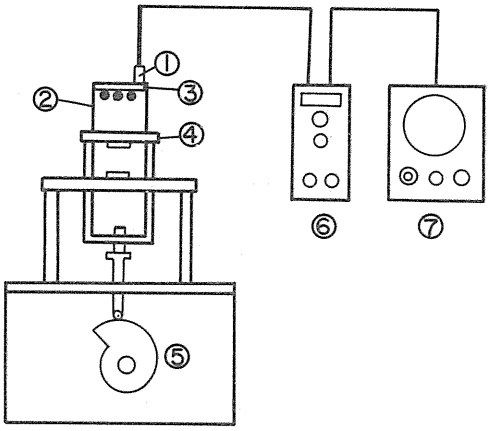

Fig. 4. 2. The experimental apparatus of impaction separation method. (① accelerometer pick-up ② cell ③ plane surface ④ tapping table ⑤ cam ⑥ amplifier ⑦ synchroscope).

the former was thought to be very suitable for the measurement at high temperature, and then this method was examined first.

4. 2. Vibration separation method

(1) Method and equipment used

As shown in Fig. 4. 1, the particles to be measured are dispersed and adhere to a plate surface (in this case glass plate) which is fixed onto a base. By giving one dimentional vibration to the base, some of the particles on it separate from the base plate by separation force caused by vibration. The separating process can be observed by a microscopy and is analyzed by micrographs which are taken before and after the separation. The adhesion force is supposed to be equal to the separation force $m\alpha\omega^2$, where the mass of a particle m is calculated from the particle size. In this experiment, the vibrating base was inclined with small angle so that the particle separated can quickly move out from the plate making the observation of separation point easier.

(2) Results and discussion

Some examples of measured results by vibration separation method are shown in Figs. 4. 3 and 4. 4. The glass beads used here were Toshiba glass beads (GB703K), from

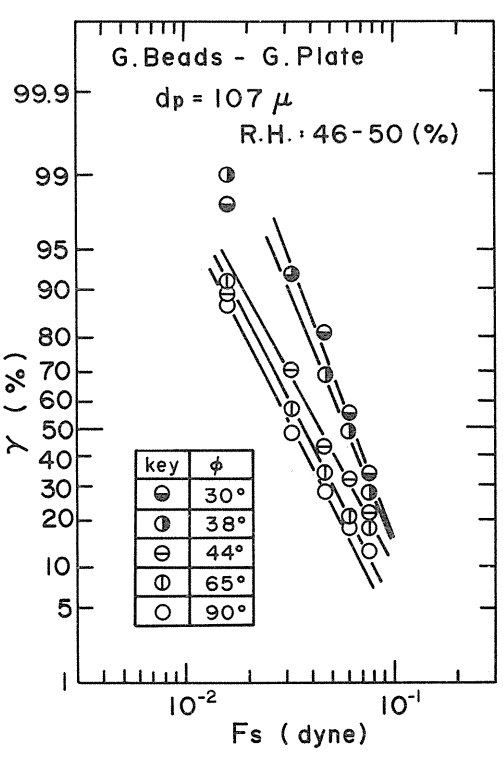

Fig. 4. 3. The results of measurement of glass beads by vibration separation method – The effect of the slope (normal separation).

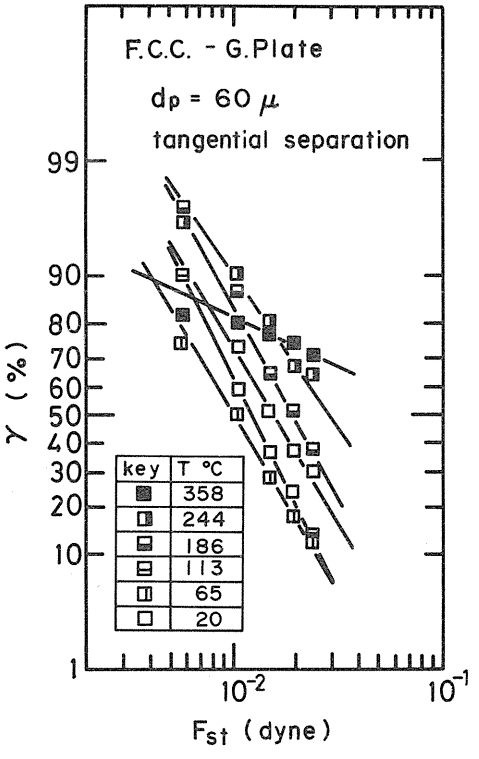

Fig. 4. 4. The results of measurement of F. C. C. particles by vibration separation method – The effect of the temperature (tangential separation).

which only the beads blocking 145 mesh screen aperture were used for the measurement. The glass plate used was micro slide glass (Matsunami Glass Industries, Ltd.) with the first grade after JIS R 3703.

The results are represented on logarithmic-normal distribution chart as the relationship between the separation force F_s as abscissa and the residual percentage of particles γ as ordinate. The relation described by the following equation, which had been reported previously by the authors[8], was reconfirmed again as shown in these figures.

$$\gamma=\frac{100}{\sqrt{2\pi}\log\sigma}\int exp\ \frac{(logF_s-log\bar{F}_s)^2}{2log^2\sigma}\ d(logF_s) \tag{4.1}$$

It had also found that the results by this method with inclined test plate always showed lower value than those by centrifugal method, and then the effect of inclination angle, ϕ, was examined experimentally. The results were obtained as shown in Fig. 4. 3. The effect of the slope angle is very clear, and it will be discussed in the following sections.

4. 3. Impaction separation method

(1) Method and equipment used

In order to extend the range of measurement, which was relatively limited in vibration separation method, an impaction separation method was developed using a measuring apparatus for which so-called tapping equipment for packing of powder bed was reconstructed and used as shown in Fig. 4. 2.

In this case, the acceleration of a particle was measured by an accelerometer pick-up (EMIC made, 509-CA type) fixed on the top of the measuring cell. As the acceleration velocity of impacted plate changed complicatedly with time, the data was taken as the peak value in the beginning period of impaction, but as the point where separation occurred was not known, this assumption should be reconsidered further. This is the weakest point of this method. Other procedure was same as vibration separation method described before.

(2) Results and discussions

With this equipment, the effect of the angle of inclination of the plane surface was again investigated. But in this case only the difference between the separation of particles from horizontal plane and that from vertical one was able to be examined, some examples of which are shown in Fig. 4. 5. In the same figure, the data with this method are compared with a datum with vibration method.

4. 4. Analysis of separation model of a particle from a plane surface

(1) Rolling model[12)13)]

A particle contacting to a plane surface can be modelled as is shown in Fig. 4. 6, where the particle adheres to a flat surface with some contacting plane, which can be approximated as a flat circle with radius a. When the separation force is exerted to the particle either by vibration or impaction acceleration, the normal component of the separation force F_{sn} acts as the main force. But the tangential component of the separation force must not be neglected, because it is impossible to give purely two dimensional vibration movement. Even in highly qualified vibrating machine, it was impossible to eliminate completely the component of right angle direction, F_{st}. This component acts as the momentum to move the particle by rotation around the bottom

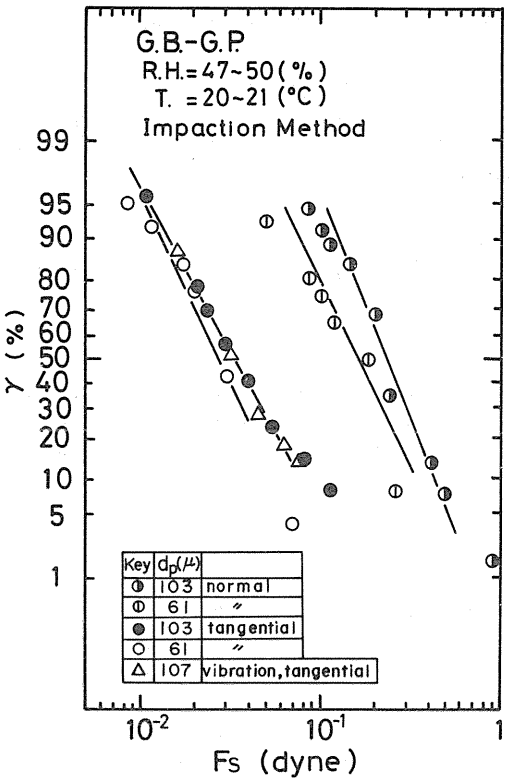

Fig. 4. 5. The results of impaction separation method comparison of normal and tangential separation.

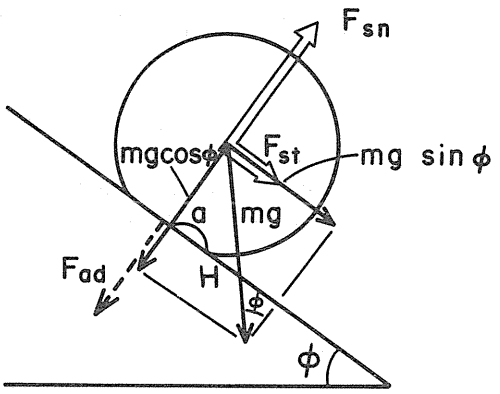

Fig. 4. 6. The model of separation of a single particle from a plane surface.

edge of the contacting plane, H. The right-angle component of gravity force to the contacting plane also acts as the rotating moment.

Accordingly, the momental balance around the point H can be expressed by the following equation taking all these forces into consideration, where the adhesion force per unit area f_{ad} is supposed to work uniformly over the contacting plane.

$$aF_{sn}+\frac{1}{2}(\sqrt{d_p{}^2-4a^2})mgsin\phi+\frac{1}{2}(\sqrt{d_p{}^2-4a^2})F_{st}$$
$$=\pi a^3 f_{ad}+amgcos\phi \qquad (4.2)$$

From the above equation, the separation force F_{sn} is obtained as follows.

$$F_{sn}=\pi a^2 f_{ad}+mg\left[cos\phi-(\sqrt{(d_p/2a)^2-1})sin\phi\right]$$
$$-(\sqrt{(d_p/2a)^2-1})F_{st} \qquad (4.3)$$

This equation shows that the required separation force F_{sn} is the adhesion force F_{ad} and other two forces indicated by the second and third terms of right hand side of the equation.

Usually contacting plane is much smaller than the diameter of the particle, then

$$\sqrt{(d_p/a)^2-1} \fallingdotseq \frac{d_p}{a} \tag{4.4}$$

Therefore Eq. 4. 3 can be written as follows,

$$F_{sn} \fallingdotseq F_{ad}+mg\cos\phi-mg\sin\phi\ \frac{d_p}{2a}-\frac{d_p}{2a}\ F_{st} \tag{4.5}$$

Only in the case of $F_{ad} \gg mg\cos\phi$, we can use this method to measure F_{ad}. Therefore

$$F_{sn} \fallingdotseq F_{ad}-mg\sin\phi\ \frac{d_p}{2a}-\frac{d_p}{2a}\ F_{st} \tag{4.6}$$

As discussed later the value of $(d_p/2a)$ is about the order of 30, and therefore when the tangential component of vibration is $10^{-2}\sim10^{-3}$ times of the normal component, this effect can not be neglected. This is the reason why the vibration to separate a particle for measurement should be strictly one-dimensional.

(2) The effect of the slope angle and its application

If we can use purely one-dimensional vibration or centrifugal or impaction separation with carefully prepared cell, the tangential component can be neglected, and then the equation can be written as follows,

$$F_s=F_{ad}-mg(d_p/2a)\sin\phi \tag{4.7}$$

The data shown in Fig. 4. 3 are conversed to fifty percent average values and plotted in Fig. 4. 7, which confirms the relation implied by the Eq. 4. 7. From the gradient of this straight line relationship in this figure, we can calculate the value of a using Eq. 4. 7. The value of a derived here is about 1.4 μm.

If this contacting plane was formed by the self weight of the particle, contacting condition can be expressed by the following Hertz's equation,

$$\left(\frac{a}{d_p}\right)^3=\frac{3}{4}\ \frac{mg(1-\nu)}{d_p{}^2E} \tag{4.8}$$

From this equation with the practical

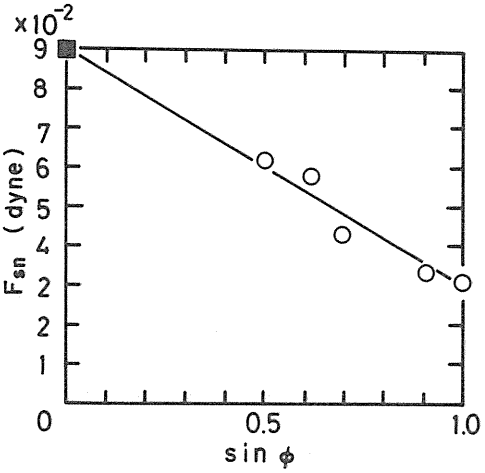

Fig. 4. 7. Relation between separation force F_{sn} and inclination ϕ with a point by centrifugal method.

data of glass (ν=0.2, E=8,000 kg/mm^2), the value of a of deformation by the self weight comes to about 23 nm for a particle of d_p=107 μm. It is much smaller than the value derived from Fig. 4. 7. Even when the additional deformation caused by the adhesion force itself is taken into account, the calculated value is very small compared with experimentally derived value.

To explain this big difference, the surface of glass beads was examined by taking photograph of scanning electron microscope, and it was found that the roughness of surface was about 5 μm. This value is well comparable to the result of a =1.4 μm above quoted.

According to the maker's information, the roughness of glass slide surface was 0.1 μm, and then if the roughness of glass beads was same as this value, the radius of imaginary contacting circle of a sphere on a plane surface at the most stable position was able to be calculated. The results were 3.2 μm for 107 μm beads and 2.5 μm for 61 μm beads. These values are also comparable enough to the results of a =1.4 μm from this experiment.

From these results it is made clear that the glass beads have a contact area having a diameter of a few micrometer with a plane surface. Then a particle can be separated with much smaller force than the force working merely in the normal direction, due to its rotating moment around the edge of contacting plane.

(3) Tangential separation method

As mentioned in the previous section, the tangential component of vibration and impaction acceleration is very effective to separate particles from plane surface, and so it would be possible to use it for the measurement of adhesion force, especially when the particle is very adhesive and the separation force is not strong enough.

In this case, where F_{sn}=0 and ϕ=90°,

$$F_{st}=(2a/d_p)F_{ad}-\left(\frac{\pi}{6}\right)d_p^{\,3}\rho_s g \tag{4.9}$$

As this method can be used only in the case that the particle can adhere to a vertical plane surface, that means that the gravity force is smaller than the adhesion force, then we can assume that $F_{st}\gg mg=(\pi/6)d_p^{\,3}\rho_s g$. Therefore the following simplified relation can be obtained,

$$F_{st}\fallingdotseq\left(\frac{2a}{d_p}\right)F_{ad} \tag{4.10}$$

From this equation, it is estimated in this case that the force required to separate a particle is only a few percentage of the adhesion force working on it. This relation was also derived by Polke[14] using different method.

In order to confirm this relation, the adhesion force was measured by the tangential separation method of vibration and impaction, and the results are shown in Fig. 4. 5 and Fig. 4. 8, which prove that the required force for the measurement by tangential method is one tenth of that by normal separation method.

Comparing these different data, we can calculate again the radii of contacting planes, and the results are a=5.6 μm from Fig. 4. 8 and Eq. 4. 9, and a=6.9 μm and 6.1 μm from Fig. 4. 5 and the same equation. These values do not correspond to those from Fig. 4. 7 and Eq. 4. 7, but are closer to the calculated values shown in the preceding section. From

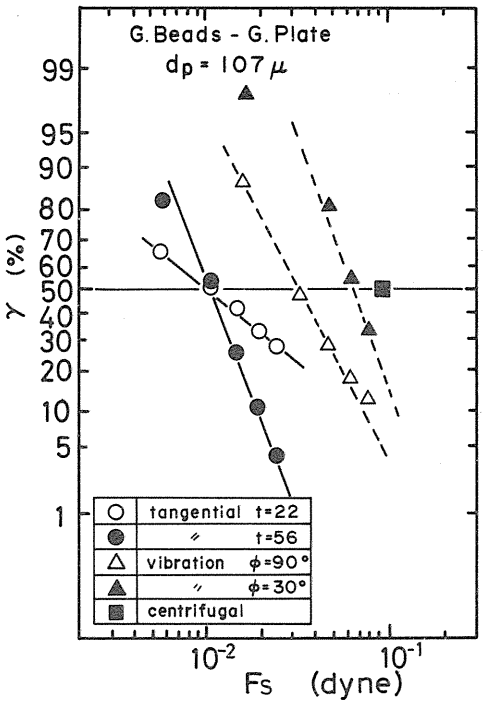

Fig. 4. 8. The results by tangential separation method, with the results by other methods.

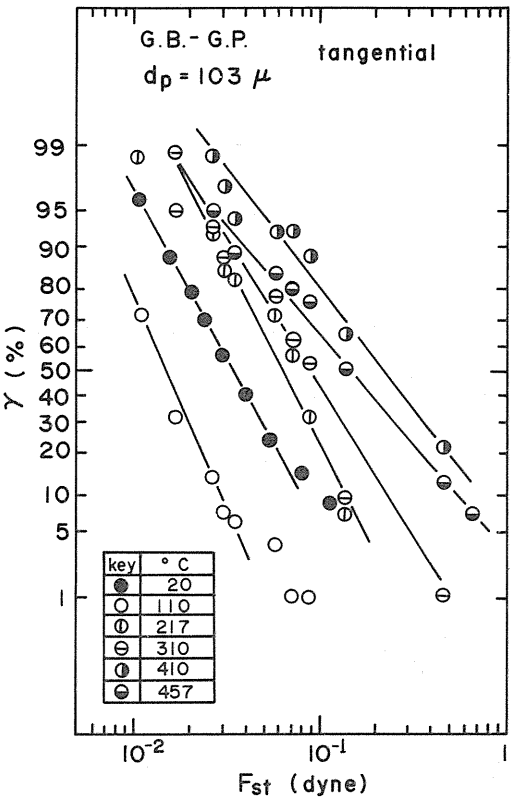

Fig. 4. 9. The effect of temperature on separation force of glass beads by impaction tangential method.

these results, we can estimate the approximate value of contacting plane at contact point between a particle and a plane surface.

Making use of this contacting relation, we developed a new tangential separation method, and it was proved that this method was effective for highly cohesive powder. We ourselves successfully applied this method to the measurement of adhesion force of particles at high temperature, as shwon in Fig. 4. 4 and Fig. 4. 9.

4. 5. Conclusions of Chapter 4

The measuring methods of single particle are already established methods, and various kinds of mechanism to separate attached particle can be applied for characterizing powder particle. And each method, namely centrifugal, vibration and impaction separation methods, has her own characteristics.

The results by these methods show that the distribution of adhesion force of powder particle is very wide. And the direction of separation force is very influential to determine the required force to separate a particle. As the separating mechanism of particle from another particle in powder assemblage might be very complicated, the direction of the force to separate it from a contacting plane surface has very wide distribution, from

normal to tangential. This factor should be taken into account to understand the behavior of powder materials.

5. Tensile strength of powder bed and the factors which control the result

5. 1. Development of new tensile strength tester[15]

5. 1. 1. Limit of Warren-Spring type tester

As was described in Chapter 3, the main problem to be solved in the measurement of powder bed was to reconsider the relation of Rumpf's equation by finding more general relationship between the adhesion force of individual particle f and the conditions of powder bed, especially porosity ε.

The split-cell type tensile tester developed by the research group in Warren Spring Laboratory, which can be characterized as No. 1 in Fig. 5. 1, has relatively narrow range of the conditions of powder bed. The most important problem was the unexpected crack formation on and in powder bed during consolidation procedure, mainly due to the uneven distribution of loading over both parts of the cell. A half of the cell on bearings is usually more unstable, and then to avoid completely the slight sink of the half cell is impossible.

Therefore to obtain the relation between porosity ε and tensile strength σ_z for sufficiently wide range, it was necessary to develop some new method. Then the authors have developed some kinds of modified Warren Spring type tester, the idea of which is to cover wide porosity range not by one single method but by two or three different methods covering different ranges.

All testers developed were horizontal type not vertical, because the vertical type tester we tested showed unstable results, perhaps the recovering of compressed powder bed could not be controlled in vertically splitting method.

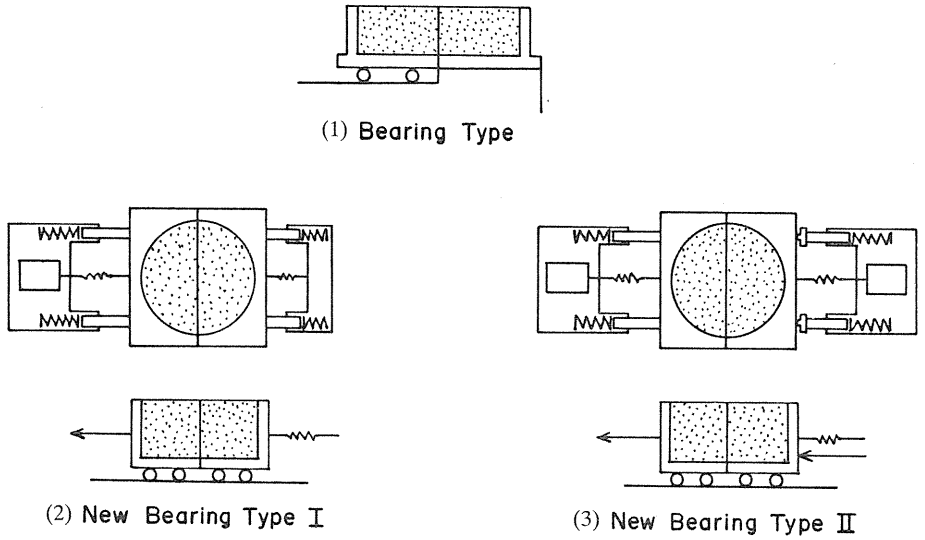

Fig. 5. 1. Comparison of the main features of bearing type testers.

5. 1. 2. Modified ball bearing methods

The first modified equipment developed by the authors is shown in Fig. 5. 2 and Fig. 5. 1 (2), in which both sides of the split cell are mounted on ball bearings. In the case of original Warren Spring type tester, one half of the cell is supported on bearings as shown in Fig. 5. 1 (1). The ideas of this modification are as follows. Firstly, both sides can move easily and therefore more accurate joining of both sides of the cell can be achieved, which avoids uneven mounting of the cell on the bearings. This unevenness was thought to be one of the main causes of unexpected crack formation in the powder bed before the cell split. And this crack formation set the limit of compression force and therefore of the porosity of powder bed.

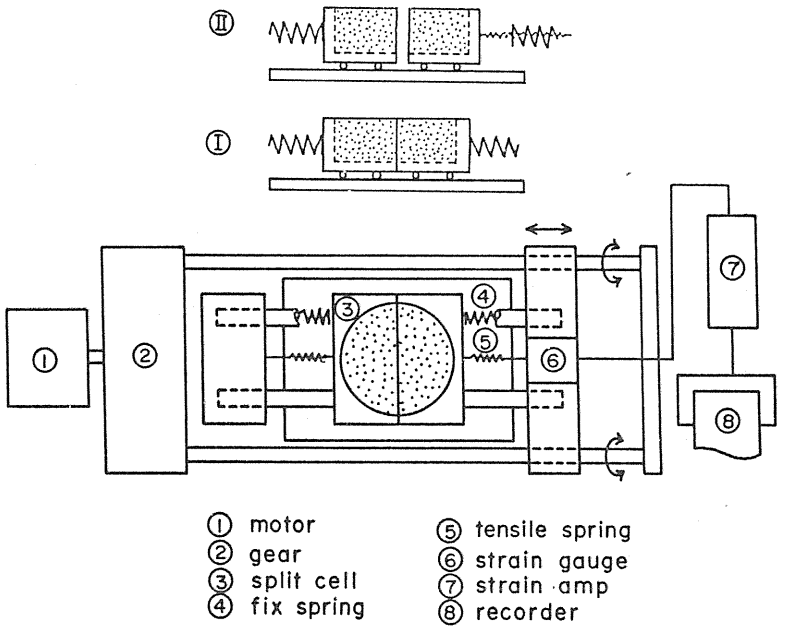

Fig. 5. 2. Modified bearing type I.

As both sides of the split cell of new equipment are mounted on ball bearings, it is necessary to have retaining rods (pushers) as are shown in Figs. 5. 1 and 5. 2. They push the cell from both sides and hold the cell tight whilst it is filled with the powder sample and consolidated. These retainers are indeed released before the sample is split by ball screws which are connected to the retainers.

Secondly, since the whole cell is movable, it is possible to split the powder bed while the cell slides. The friction of the bearings is thus reduced, and the consequent reduced tare value increases the accuracy of measurement, especially in high porosity range. Additionally, there is a possibility to eliminate the need to measure the tare value of friction, if the tensile tension of both sides can be measured.

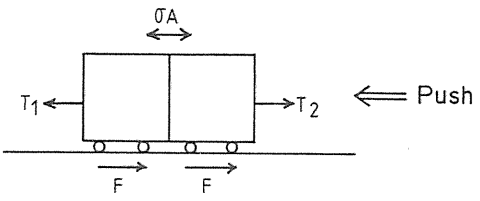

Fig. 5. 3. Balance of force in split-in-slide method.

This so-called split-in-slide method can be explained with Fig. 5. 3 as follows; The balance of forces in the moving cell is

$$T_1 - 2F - T_2 = 0 \tag{5.1}$$

And the balance of force at the failure point is

$$T_1 - F = \sigma_z A \tag{5.2}$$

From these equations,

$$\sigma_z = \frac{T_1 + T_2}{2A} \tag{5.3}$$

But with this equipment, it was very difficult to move the cell steadily, because to pull it by a spring against another spring tension frequently caused unsteady vibration. Therefore another mechanism to improve this point had to be introduced, and then second modified equipment was developed as shown in Fig. 5. 4. In this new equipment, another "pushing" mechanism was introduced. Four pushers from both sides retain the split-cell joint while the cell is filled with powder and the powder bed is consolidated. Then the pushers release the cell by removing the "pushers" on one side, which move faster than the others as are indicated in Fig. 5. 4 as 50 mm/min and 20 mm/min as examples. The "pushers" on the other side continue the motion of the cell with slower speed to the same direction of splitting. Therefore the cell on bearings moves steadily at the same speed of the slower pushers. Then the tension from the spring connected to faster "pushers" via strain gauge gradually increases until the powder bed in the cell splits. The cell can then slide only against dynamic friction, which is smaller than static.

In the modified split-cell type equipments, the tare values of friction reduced largely

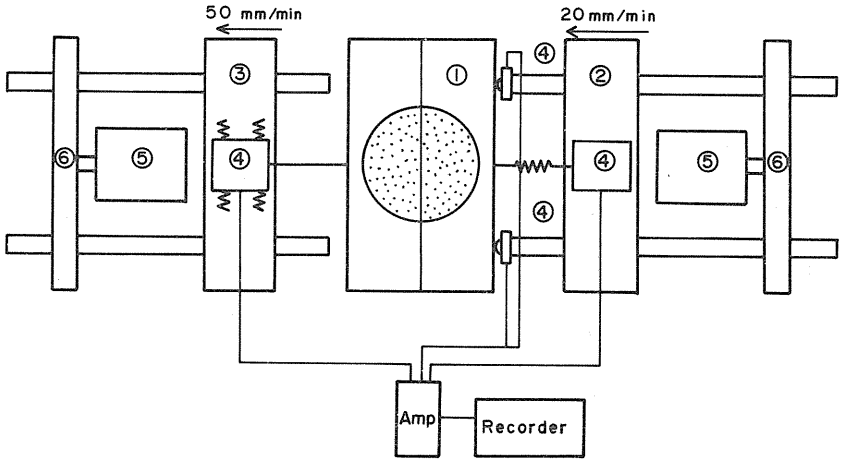

Fig. 5. 4. Modified bearing type II.

compared with the original type tensile tester, and then the limit of measurement was able to be shifted to more loose packing side.

5. 1. 3. No bearing method

For measurement in highly compacted range, it is not essential to reduce the friction of the bearings but the stability of the cell during consolidation procedure is most important. Therefore, in the third modification of the split cell method, all ball bearings were eliminated and one half of the cell was placed on the flat surface of the base, as shown in Fig. 5. 5. A solid lubricant, such as MoS_2, was used to reduce the friction of the contacting flat surfaces.

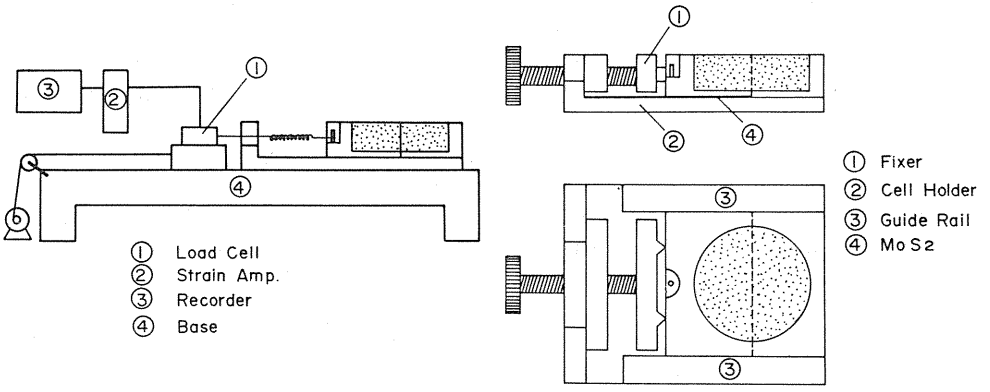

Fig. 5. 5. No-bearing type tensile tester.

Without ball bearings, an increased value of the friction was unavoidable, as shown in Table 5. 1, but the cell became very stable, even during the consolidation of powder bed by high loading, and therefore the scatter of the data obtained became very small. The tare values of the friction for the cell in each type of equipment and the possible range of consolidating loads for the powder bed are also summarized in Table 5. 1.

In addition to these three modified methods, another commercially available equipment, "cohetester", was also used[16] in which half of the cell is suspended by three leaf springs in place of ball bearings.

Table 5. 1. Friction of sliding of cells and the ranges of consolidating load.

Type of equipment	Tare value of friction $\times 10^2$ [N]	Range of consolidating load [kPa]
Warren Spring Type	2.5 ~ 6	1 ~ 25
Modified Bearing Type I	1 ~ 2	0 ~ 50
Modified Bearing Type II	0.3 ~ 0.4	0 ~ 50
No Bearing Type 1	12 ~ 16	5 ~ 5000
No Bearing Type 2	30 ~ 40	5 ~ 10000

5. 2. Experimental method and materials tested

5. 2. 1. Experimental procedure and materials

Following experiments were achieved by using four tensile testers described in the preceding section. The experimental procedure is the same in all four types of tester, though the details were slightly different each other.

In the modified bearing type testers, the cells were always mounted on the ball bearings while being filled with sample powders and while the powders were consolidated. But in the "no bearing" type of tests, the split cell was fixed tightly with cell holder, as shown in Fig. 5. 5, and then the holder itself with the cell was able to be removed from the base of the tester for putting into an ordinary press for consolidating and for pressing with high loading, and also, if necessary, to put on a tapping machine to compact the powder bed.

During filling and consolidating, the both sides of the cell were cramped with cylindrical outer case which was higher than the cell itself, so that it did contain excess sample powder. The amount of excess powder was so selected that the height of excess powder over the edge of the cell wall was always roughly the same. This was to keep the consolidation pressure through powder bed over the cell onto the powder bed in the cell constant.

The dimensions of the cell was 50mm inner diameter and 20mm depth. The bottom surface was roughened with sand paper to avoid the slippage with powder bed.

Consolidation by loading was usually 10 min, which was determined by preliminary tests. But even after 10 min, there still existed gradual and small increase of consolidation.

After that, the bulk volume of the samples in the cell was maintained precisely constant by scraping off the excess powder over the edge of the cell with a sharp straight blade. The porosity of the bed was thus accurately calculated by weighing the mass of the powder sample after splitting the powder bed.

In the extremely compacted range, it was sometimes necessary to place two small wires vertically on the inner wall of the cell, close to the vertical splitting face in order to avoid the formation of an irregular failure face in the powder bed. In following figures, this special type of the cell will be denoted as "special cell".

The materials mainly tested in this experiment are shown in Table 5. 2. The powder samples were kept in a desiccator for more than one week in order to maintain the moisture content within a certain range.

Table 5. 2. Characteristics of powders tested.

No.	Sample materials	Average size [μm]	Density of powder particles $\times 10^{-3}$ [kg/m^3]
1	Limestone powder (P-30)	5.6	2.7
2	Limestone powder (P-70)	19.6	2.7
3	Fused alumina powder (W.A. #2500)	6.2	3.9
4	Lactose	46.9	1.5
5	Loam clay powder (Kanto loam, JIS Z8901 – No. 11)	2.0	3.0

5. 2. 2. Experimental results

Some examples of the results of measurement of typical materials are shown in Fig. 5. 6 as the relation between the tensile strength of powder bed, σ_z, and the porosity, ε. The types of equipment used are also shown in this figure. Connecting the results by several different methods, then we can obtain the wide range of the relationship between above mentioned factors.

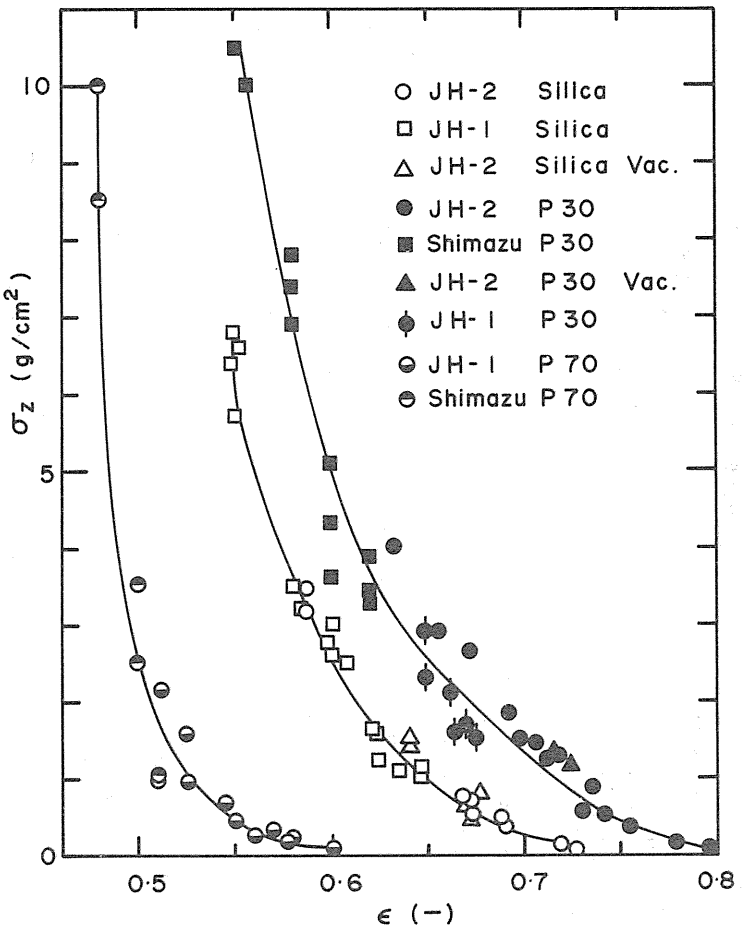

Fig. 5. 6. Relationship between the tensile strength and the porosity of powder bed (JH denotes the results by the testers in Table 5. 1).

It was found that this relation was able to be represented by semi-logarithmic relation as shown in Fig. 5. 7.[17] The relation was proved fairly well, and therefore now all results

by the authors are represented by this relation as follows,

$$\sigma_z = k_1 exp\left(-\frac{\varepsilon}{b}\right) \tag{5.4}$$

Other data collected by the working party on powder mechanical properties (led by Prof. A. Ohtsuka) organized by the Society of Powder Technology were correlated with the same relation successfully.[18] But this relation does not correspond to the relation of Rumpf's equation. This is very interesting because Rumpf's model bases on the model of particle packing which is assumed to be homogeneous structure, whereas Eq. 5. 4 describes the strength of powder bed based on the probabilistic model of failure phenomenon, which corresponds to the fact that the crack formation usually starts from the surface, where the weakest points distribute.

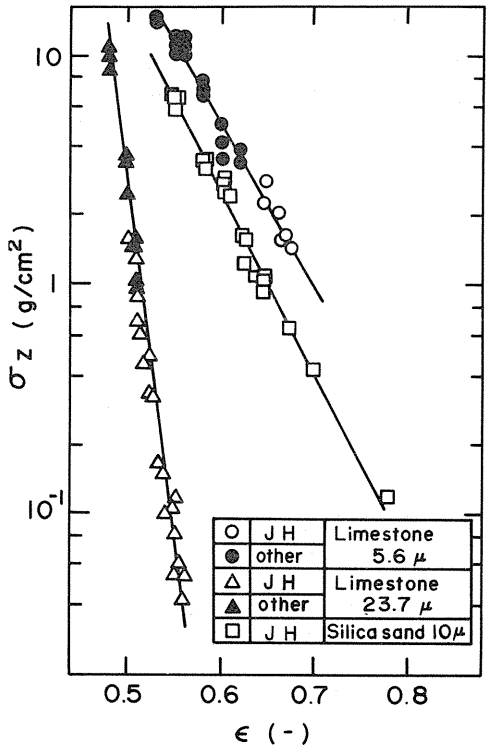

Fig. 5. 7. The results of measurement of modified bearing method.

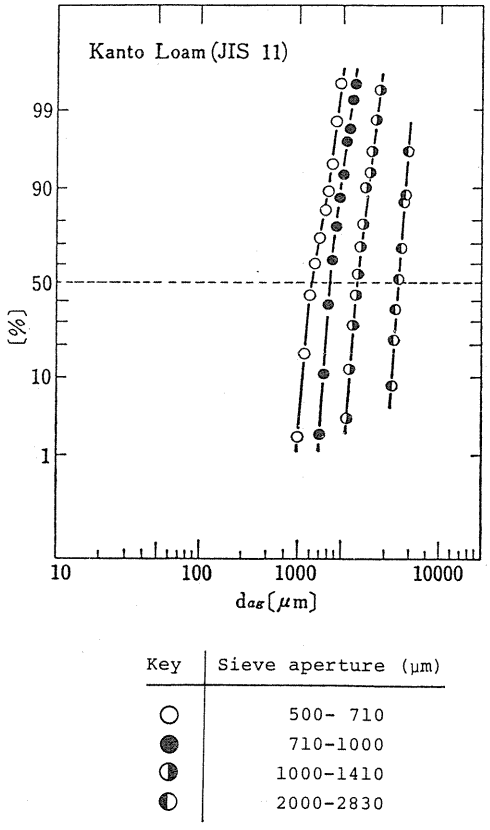

Fig. 5. 8. Size distribution of agglomerated powder particle through sieves.

5. 2. 3. The factors which control the tensile strength of powder bed

(1) The effect of powder bed formation[19)]

For investigating the effect of various factors which control the tensile strength of powder bed, the effect of the structure of powder bed was examined first.

In this case, the sample powder was fed into the cell with two ways, the first one was with a spatula and the second was through sieves. By changing the sieve aperture, the size of agglomerated powder changed as one example was shown in Fig. 5. 8. The size of the agglomerate was measured with image analysis and the Feret's diameter was taken as representative value. The density of the agglomerates was measured by weighing them and calculating from sphere particle assumption.

The results by a cohetester are shown on semi-logarithmic chart as indicated in Figs. 5. 9, 10 and 11. In the case of relatively cohesive powder such as clay (Kanto loam

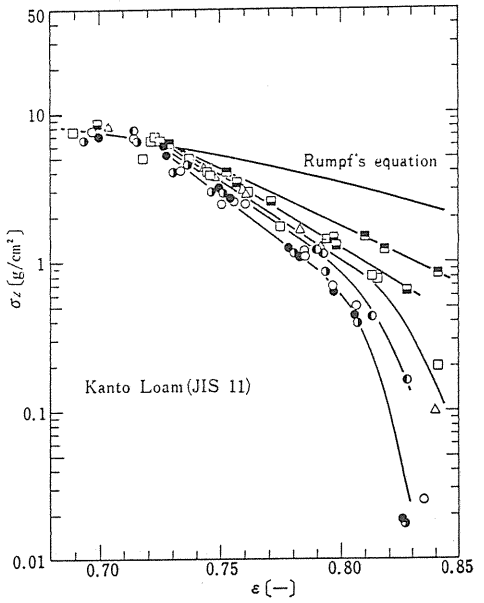

Key	Sieve aperture (μm)
▣	- 63
■	- 350
□	-1000
○	500- 710
●	710-1000
◑	1000-1410
◐	2000-2830
△	Feed with Spatula

Fig. 5. 9. Relationship between the tensile strength σ_z and the porosity ε (Kanto loam clay).

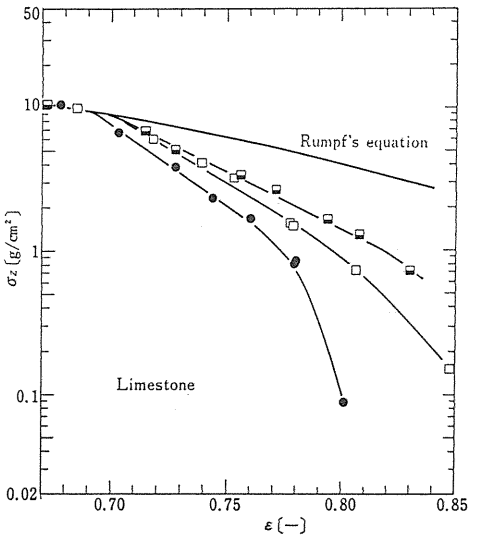

Key	Sieve aperture (μm)
■	- 350
□	-1000
●	710-1000

Fig. 5. 10. Relationship between the tensile strength σ_z and the porosity ε (Limestone).

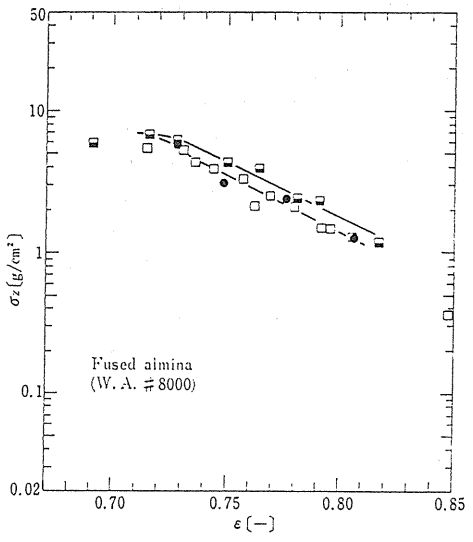

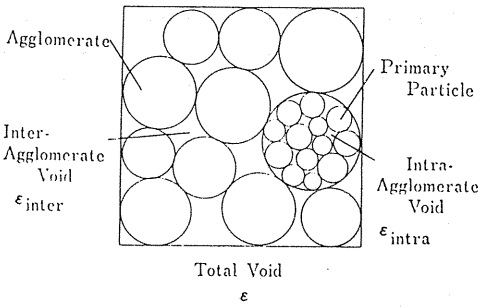

Key	Sieve aperture (μm)
■	- 350
□	-1000
●	710-1000

Fig. 5. 11. Relationship between the tensile strength σ_z and the porosity ε (Fused alumina powder).

Fig. 5. 12. The packing model of primary and secondary particles.

powder) and limestone, there appeared the effect of the agglomeration. When the size of agglomerates increased, the value of σ_z decreased, and especially in very loose state, the deviation from the straight line relationship was very clear.

In the case of non-cohesive materials such as fused alumina powder, there was no such a distinct shift of the line. Therefore it was obvious that the formation of agglomerates in powder bed caused the drop of the strength.

It was also found that when the porosity decreased or consolidation pressure increased, the straight line with different agglomerations approached to a sort of starting point, and then below a certain porosity all values of tensile strength with different conditions became the same.

This fact can be explained by the disappearing of the agglomerates due to high load compression. The model of this powder bed structure is shown as Fig. 5. 12.

Figs. 5. 13 and 14 show the change of inter-agglomerate voidage, which was calculated from the value of bulk density of the agglomerates. These results show that at certain compression pressure, the agglomerates disappear. And these values well correspond to the values of the starting point on $\sigma_z \sim \varepsilon$ relationship.

Another important finding related to the effect of powder bed formation is direct

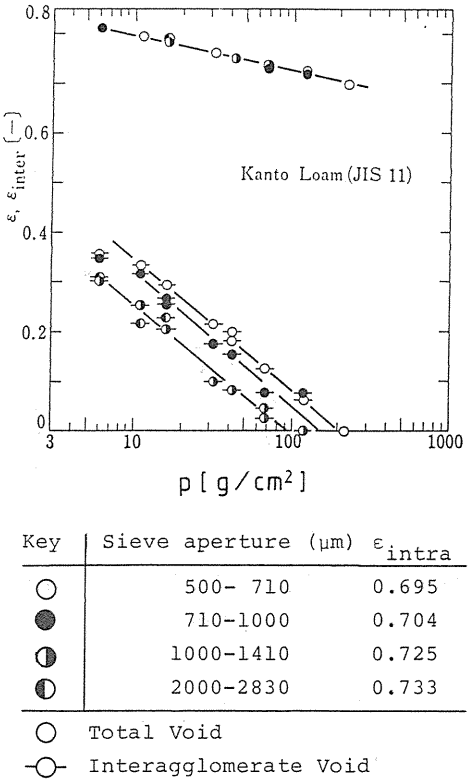

Fig. 5. 13. Relationship between pre-compression stress and the change of the total and the inter porosity of powder bed (Kanto loam clay).

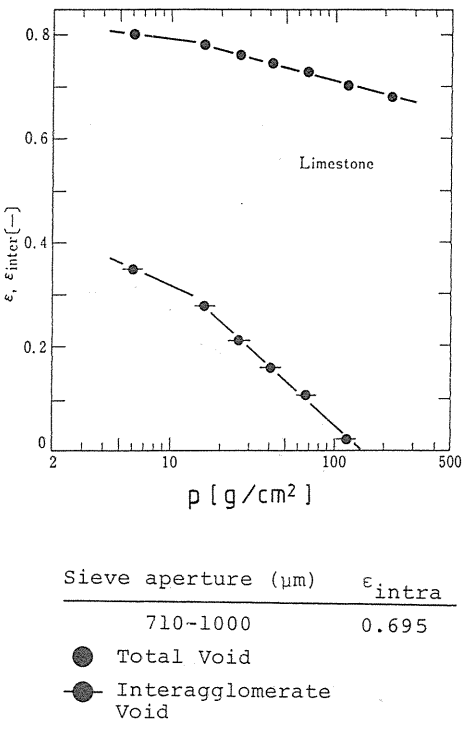

Fig. 5. 14. Relationship between pre-compression stress and the change of the total and the inter porosity of powder bed (Limestone powder).

effect of compression stress p on the tensile strength, σ_z. Figs. 5. 15, 16 and 17 show the relationships between the bed strength and the compression stress to form the bed. In the case of non-cohesive powder like fused alumina powder, it can be shown as one straight line irrespective of the size of agglomeration, whereas in the case of cohesive powder the agglomeration may affect to this relation, but that effect is much smaller than that in the relation of ε and σ_z above described. Based on this experimental results, we proposed the following equation which also characterized the cohesiveness of powder.

$$\sigma_z = k_2 p^m \tag{5.5}$$

This equation points out the importance of pre-consolidation process, which one of the authors has already pointed out in conjunction with the comparison between compression and tapping of powder bed.[9)]

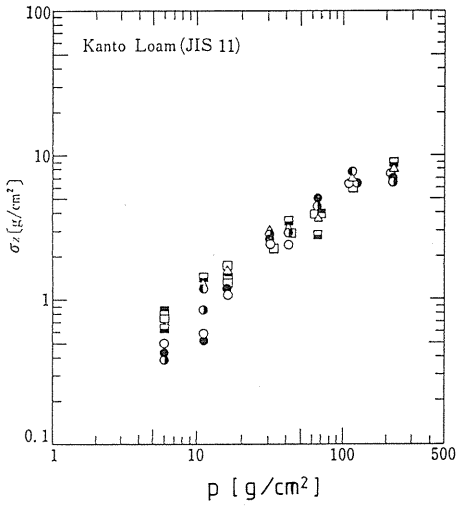

Key	Sieve aperture (μm)
▣	- 63
▣	- 350
□	-1000
○	500- 710
●	710-1000
◑	1000-1410
◐	2000-2830
△	Feed with Spatula

Fig. 5. 15. Relationship between pre-compression stress and the tensile strength (Kanto loam clay).

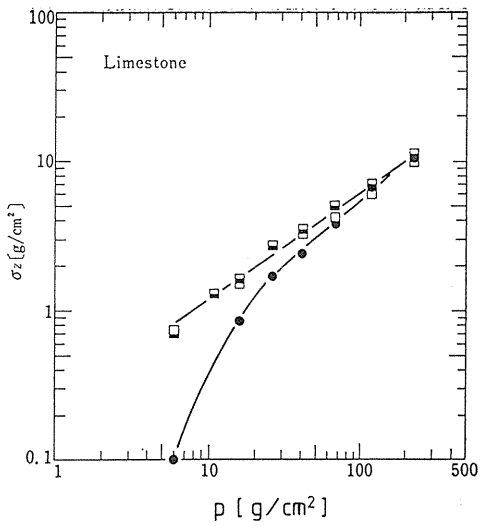

Key	Sieve aperture (μm)
▣	- 350
□	-1000
●	710-1000

Fig. 5. 16. Relationship between pre-compression stress and the tensile strength (Limestone powder).

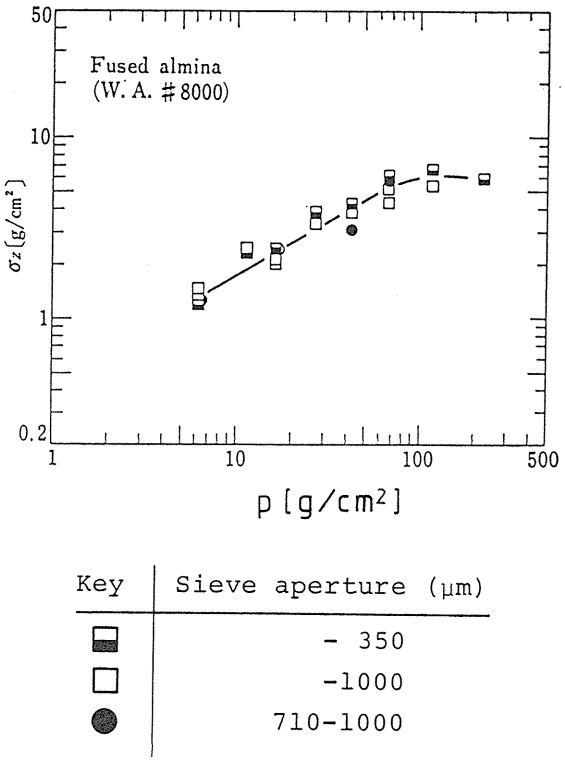

Fig. 5. 17. Relationship between pre-compression stress and the tensile strength (Fused alumina powder).

(2) The effect of particle size and powder properties

The relationships between the tensile strength and the other factors of powder bed, proposed in the preceding section, were examined by changing the surface property of particle. Anhydrous silica was used as an additive to improve mechanical powder properties.[20]

The relationships between the tensile strength and the porosity or the compression stress are shown in Figs. 5. 18 and 19, and Figs. 5. 20 and 21.

Besides the effect of additive, of which the discussion was made in the other papers,[21][22] these results clearly prove the relations of Eqs. 5. 4 and 5. 5. But in this case, the relation between σ_z and p was not simple as was expected from Figs. 5. 15, 16 and 17. Perhaps this is due to the change of compression stress transfer by adding this kind of lubricating material. But this problem was left for further investigation.

5. 3. *Derivation of semi-theoretical equation of the strength of powder bed*[23]

As described hitherto in this paper, the relationship expressed by Eq. 5. 4 was proved in a fairly wide porosity range (Fig. 5. 22), except when the agglomeration phenomenon occurred.

And also the relationship expressed by Eq. 5. 5 was proved very extensively (Fig. 5. 23). Now the problem is to find out the relation between these two relations.

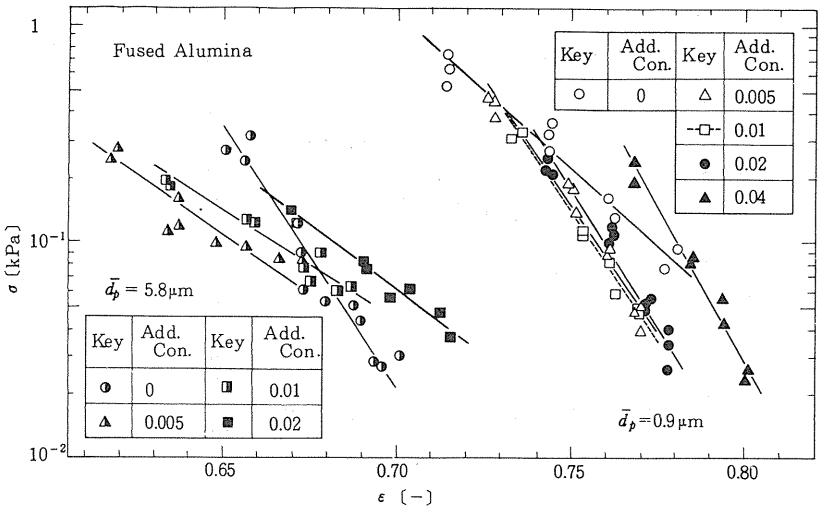

Fig. 5. 18. Relationship between tensile strength and porosity of powder bed (Fused alumina powder).

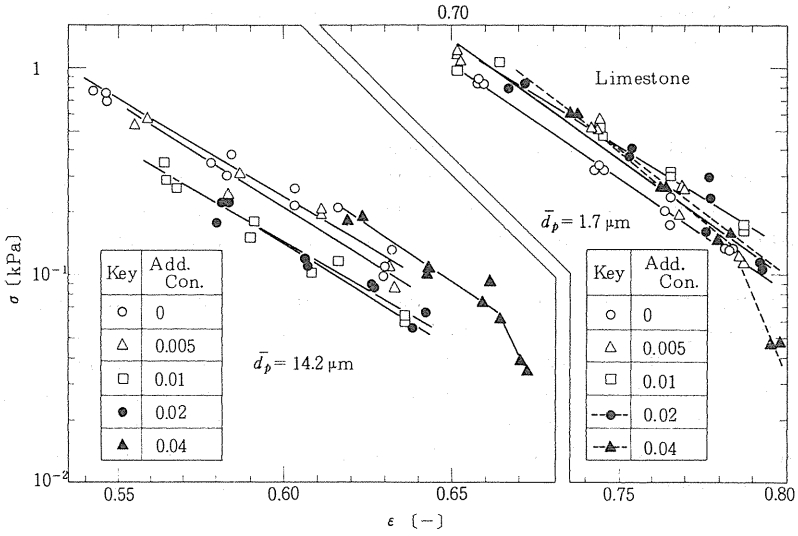

Fig. 5. 19. Relationship between tensile strength and porosity of powder bed (Limestone).

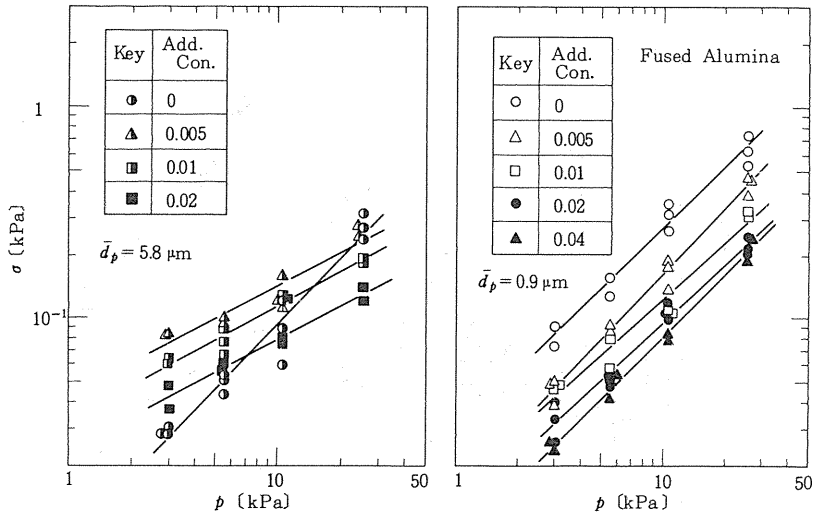

Fig. 5. 20. Relationship between tensile strength and pre-compressive stress (Fused alumina powder).

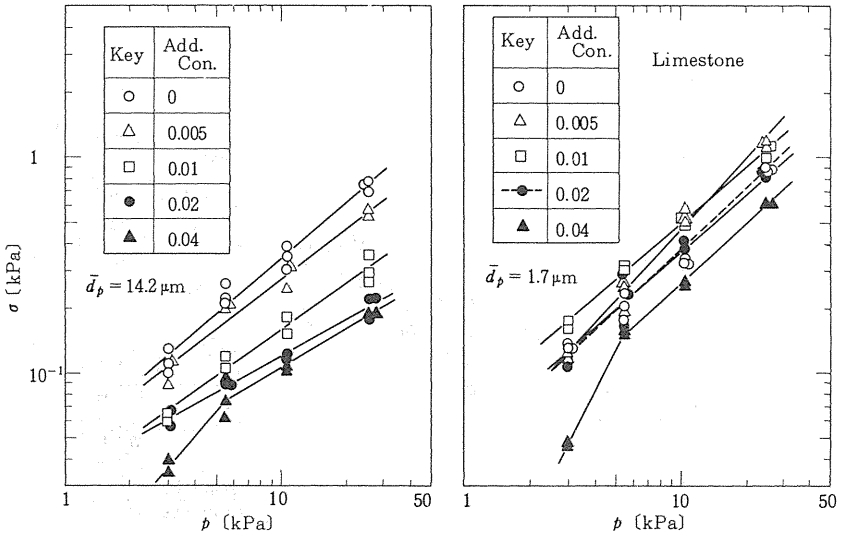

Fig. 5. 21. Relationship between tensile strength and pre-compressive stress (Limestone).

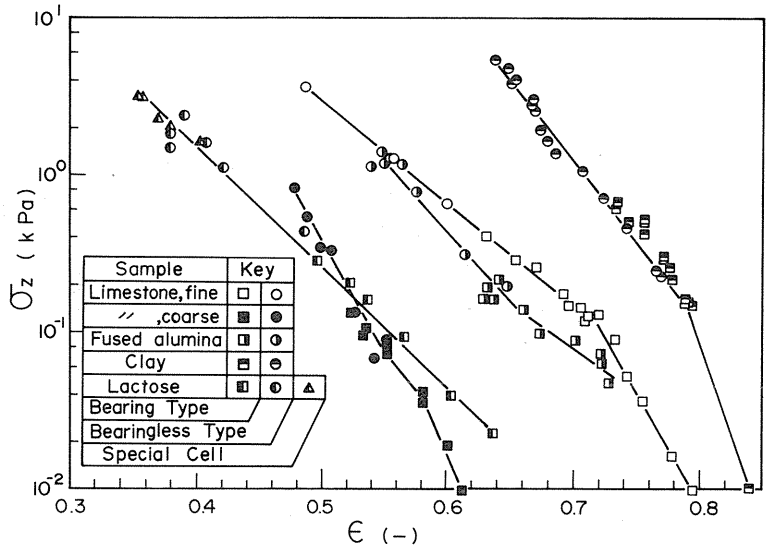

Fig. 5. 22. Summarized results of the tensile strength and the porosity of powder bed represented on semi-logarithmic chart.

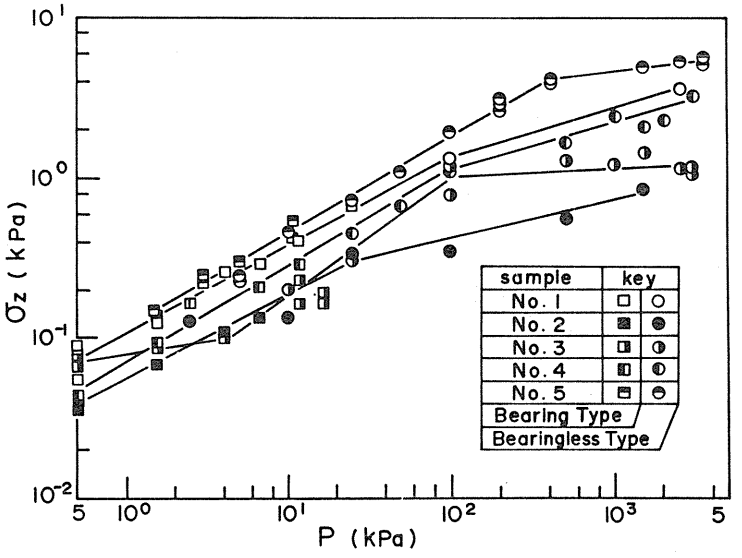

Fig. 5. 23. Relationship between compressive stress and tensile strength.

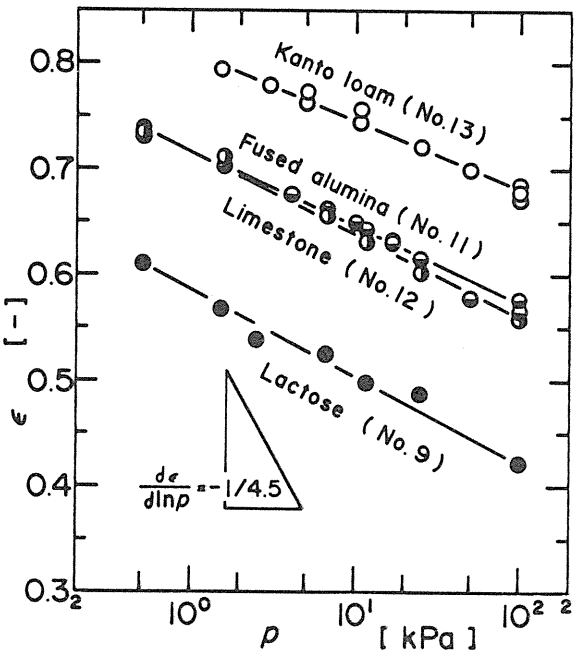

Fig. 5. 24. Summarized representation of the relationship between the porosity of powder bed and the compressive stress on semi-logarithmic chart.

There is also the relation between the compression stress and the porosity. It was derived as the following equation from the experimental results described in the preceding section and shown here (Fig. 5. 24). This relation has widely been accepted as a general equation for powder packing process,

$$p = k_3 exp\left(-\frac{\varepsilon}{c}\right) \tag{5.6}$$

where k_3 and c are constants as usual.

Then the following equation can be deduced by substituting Eq. 5. 6 into Eq. 5. 5.

$$\sigma = k_2 k_3^m exp\left(-\frac{m\varepsilon}{c}\right) \tag{5.7}$$

From the comparison of Eq. 5. 4 and Eq. 5. 7, the following relations are obtained:

$$k_1 = k_2 k_3^m \tag{5.8}$$

$$b = \frac{c}{m} \tag{5.9}$$

If Eqs. 5. 8 and 5. 9 are confirmed experimentally, Eq. 5. 4 can be derived from Eqs. 5. 5 and 5. 6.

On the other hand, Rumpf[24] has derived the following famous equation.

$$\sigma=\frac{1-\varepsilon}{\pi}k\frac{F}{d_p^2} \tag{5.10}$$

As the tensile strength of a powder bed, where k, d_p and F are the average coordination number, the particle diameter and the adhesion force at the contact point of particles, Nagao[25] analysed the stress-strain relations of granular materials theoretically and derived the same equation in general form. Molerus[26] also derived the same result in his theoretical research concerning the yield of cohesive powders. Furthermore, Kanatani[27] derived a general equation being coincident with Rumpf's equation.[28][29]

Accordingly Eq. 5. 10 can be used as the general equation of the relation of stress and force at the contact point of particles, irrespective of the direction of stress-tensile, compressive or shear.[30]

If we assume $k\varepsilon=\pi$, Eq. 5. 10 becomes following equation, as Rumpf proposed long before.

$$\sigma=\frac{1-\varepsilon}{\varepsilon}\frac{F}{d_p^2} \tag{5.11}$$

This equation can be transformed into a practical equation by introducing the following approximation, which the authors have found to be applicable in the porosity region of about 0.4 ~0.9.

$$\frac{1-\varepsilon}{\varepsilon}=10exp(-4.5\varepsilon) \tag{5.12}$$

Then the following practical equation can be obtained,

$$\sigma=10exp(-4.5\varepsilon)\frac{F}{d_p^2} \tag{5.13}$$

By using the modified equation of generalized Rumpf's equation, the adhesion force F will be correlated to the pre-compressive force P. F can be calculated by Eqs. 5. 4 and 5. 13 as follows:

$$F=0.1k_1d_p^2exp\{(4.5-\frac{1}{b})\varepsilon\} \tag{5.14}$$

P can also be calculated by Eqs. 5. 13 and 5. 6 as follows:

$$P=0.1k_3d_p^2exp\{(4.5-\frac{1}{c})\varepsilon\} \tag{5.15}$$

Therefore, the relation of the adhesion force F and the pre-compressive force P is obtained as follows, by eliminating the porosity ε from Eqs. 5. 14 and 5. 15.

$$F=10^{n-1}k_1k_3^{-n}d_p^{2(1-n)}P^n \tag{5.16}$$

where

$$n=\frac{(4.5-1/b)}{(4.5-1/c)}$$

On the other hand, the tensile strength σ and the pre-compressive stress p in Eq. 5. 5 are transformed into the adhesion force F and pre-compressive force P respectively by Eq. 5. 11. And also the following assumption can be made

$$\varepsilon^{1-m}(1-\varepsilon)^{m-1}\fallingdotseq 1.0$$

and then the following equation is obtained:

$$F=k_2d_p^{2(1-m)}P^m \tag{5.17}$$

If this relation, expressed as Eq. 5. 17 derived from Eq. 5. 5, can be confirmed by experimental data, it is now possible to say that the relation of Eq. 5. 5 explains the relationship between the pre-compressive force and the adhesion force at the interparticle contact point.

Accordingly we propose here the new equation

$$\sigma=\frac{1-\varepsilon}{\varepsilon}k_2\frac{P^m}{d_p^2} \tag{5.18}$$

as the semi-theoretical equation expressing the tensile strength of a powder bed.

5. 4. Experimental verification of derived semi-theoretical equation and discussions

From the results of the measurement of tensile strength of powder materials, the values of b, c, and m are shown for comparison in Table 5. 3.

First the relations of Eqs. 5. 8 and 5. 9 were proved as shown in Figs. 5. 25 and 26 respectively.

Secondly about the values of b and c, the following considerations can be done. The relation of σ_z and ε in Eqs. 5. 6 and 5. 13 is represented schematically as Fig. 5. 27.[30] When the powder bed with porosity ε_0 and strength σ_{z0} is compressed to porosity ε_1 with compressive stress p, the increase of σ_z will be made along the straight line up to σ_z. When the adhesion force F is constant irrespective of porosity, the slope of this line should be $-1/4.5(=0.222)$ according to Eq. 5. 13. Therefore in Fig. 5. 27, the increase of the strength is shown as $\ln\sigma_z'-\ln\sigma_{z0}$, which is simply due to the increase of interparticle contact points, as Rumpf's equation assumed.

But real increase of the strength is $(\ln\sigma_{z1}-\ln\sigma_{z0})$ and the slope of this straight line is $-1/b$. As is shown in Table 5. 3, the value of $-1/b$ is always much larger than -4.5, and naturally $(\ln\sigma_{z1}-\ln\sigma_{z0})$ is larger than $(\ln\sigma_z'-\ln\sigma_{z0})$. Therefore this increase of the strength,

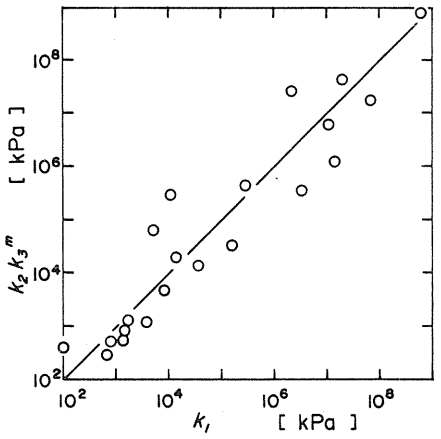

Fig. 5. 25. The relationship between $k_2k_3^m$ and k_1.

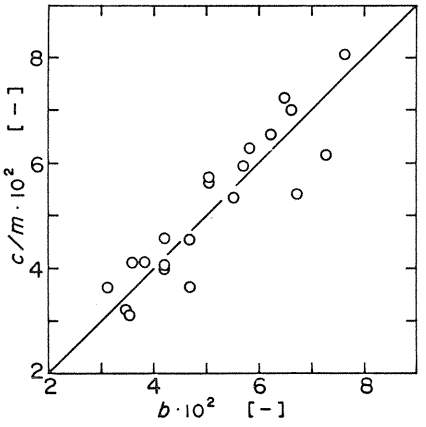

Fig. 5. 26. The relationship between c/m and b.

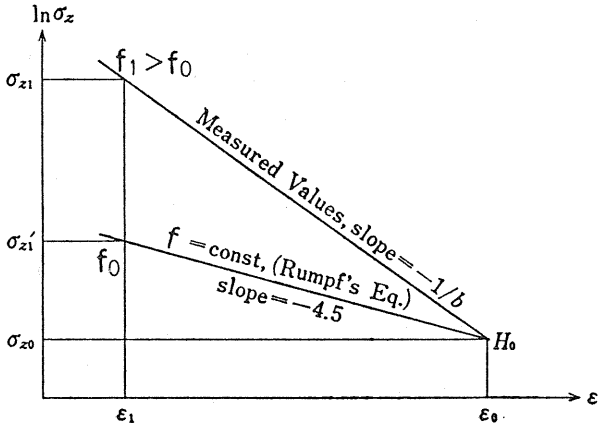

Fig. 5. 27. Analysis of tensile strength test.

$(\ln\sigma_{zl}-\ln\sigma_{zl}')$, is not due to the increase of the number of contact point, but due to another factor, namely the increase of adhesion force at contact point. And it was found that the latter was usually several times larger than the former. This is the main reason why Rumpf's formula should be modified, and the conditions of formation of powder bed is more deterministic than the simple decrease of porosity.

Table 5. 3 Used sample powders and experimental results of some characteristic values.

No.	Sample Powder	d_{pl} [μm]	$b\times10^2$ [−]	$c\times10^2$ [−]	m [−]
1	Kanto loam	2.0	4.21	2.91	0.718
2	Kanto loam	2.0	4.21	2.74	0.602
3	Kanto loam	7.0	5.04	3.78	0.582
4	Kanto loam	30.0	3.60	1.17	0.285
5	Agg. of K. L.	2.0	3.47	3.04	0.948
6	Limestone	1.7	4.21	2.87	0.718
7	Limestone	5.6	5.82	3.78	0.602
8	Limestone	5.6	6.73	3.47	0.643
9	Limestone	19.4	3.13	1.87	0.515
10	Agg. of L. S.	1.7	3.82	3.78	0.917
11	Fused alumina	1.3	5.52	2.74	0.512
12	Fused alumina	6.2	7.64	3.17	0.392
13	Lactose	46.9	5.69	3.58	0.602
14	Smokeless coal	34.0	5.03	2.52	0.448
15	Weak-coking coal	30.0	4.69	2.69	0.737
16	Non-coking coal	33.0	4.69	3.34	0.737
17	Brown coal	32.0	3.54	1.39	0.448
18	Fly ash (0.3 %)*	11.8	5.07	1.52	0.270
19	Fly ash (0.54%)	11.8	7.28	1.93	0.314
20	Fly ash (0.77%)	11.8	6.49	2.87	0.397
21	Fly ash (1.0 %)	11.8	6.62	2.98	0.426
22	Fly ash (1.3 %)	11.8	6.24	3.32	0.507

* Percentage denotes the value of water content

The same procedure can be made for obtaining the value of c. Again the slope of straight line in Fig. 5. 24 can be obtained from Eq. 5. 15, because this equation is written as follows.

$$p=10exp(-4.5\varepsilon)\frac{P}{d_p^2} \tag{5.19}$$

And therefore the slope should be $-1/4.5$, and again this is much larger than the values experimentally obtained as shown in Table 5. 3. This fact shows that the increase of compressive stress causes the increase of compression force at the contact point of

particles, then that force increases the interparticle adhesion force when the particles are split.

5. 5. Conclusion of Chapter 5

To investigate the measurement method of tensile strength of powder bed, several principles and techniques have been developed by the authors, and with these equipments the tensile strength of powder bed was able to be measured for fairly wide range of porosity, and therefore the relationships between the tensile strength and the other factors of powder bed were obtained. Especially the relationships between the tensile strength and the porosity was found to be expressed by an exponential equation.

Then the fundamental equation was derived semi-theoretically to obtain a modified Rumpf's equation, in which the compressive force at the contact point of particles was included as an important factor. That equation shows that the increase of the strength of powder bed is not only by the increase of the number of contact point but also by the increase of compressive force at contact point.

Therefore the method to make a powder bed is very important controlling factor of the strength of powder bed to test. And as the compressive stress can be varied in very wide range, the strength of powder bed to be tested with the same porosity may vary largely.

6. Measurement of the strength of powder agglomerates

6. 1. Failure of agglomerate of powder in flow field

In chemical engineering processes, many powders are treated in flow field. As was pointed out by the authors[31] and other powder scientists, powder particle has "equilibrium diameter", which is defined as the diameter of the particle whose adhesion force at the contact point with other solid surface is the same as its gravity force. And as the adhesion force is thought to be proportional to the diameter, and the gravity force is proportional to the cubic of the diameter, the adhesion force of the particle smaller than the equilibrium diameter becomes controlling factor compared with the gravity force. In the case of mineral particles such as silicate sand and limestone, that equilibrium diameter is about 50μm, or perhaps from 20μm to 70μm. Therefore below that size, particles tend to stick each other and to form permanent agglomerate which behaves as a single particle.

In fluid flow, especially in gas flow, the drag force is usually almost equivalent to the gravity force, and then the agglomerate is stable. Therefore in many powder processes, this agglomerate should be treated as a particle, and so the adhesiveness of solid particle is very effective in many unit operations such as classification.[32]

On the other hand, the measured results of the adhesion force of particles related to air flow phenomena all showed very small values compared with other methods described in the preceding two chapters as were shown in Chapter 3, Fig. 3. 1, and so it was necessary to develop some specific method to measure the adhesiveness of powder in air flow.

6. 2. Mechanism of the failure of agglomerates in air flow field

6. 2. 1. Empirical relation proposed

To investigate the mechanism of breaking down process of agglomerated powder in air flow, there had been proposed and developed several kinds of measuring methods, which can be classified as follows.

(1) Collision with some solid obstacles[33][34]

(2) Fluid dynamic force, or impaction or shearing by air flow
   a. Acceleration (Injection or capillary)[35)36)]
   b. Deceleration

First, one of the authors adopted acceleration method using long horizontal tube into which agglomerated powders were fed and the air flow accelerated them very quickly.[37)] It was successful to break the agglomerates and to characterize qualitatively the adhesiveness of powder, and the author proposed the following equation to characterize the dispersability of powders.

$$d_{ag} \cdot u_r^{\,m} = const. \tag{6.1}$$

In this case, relative velocity u_r is approximated with the velocity of air flow in the pipe.

The value of m has been obtained by several workers by different methods, which are summarized in Table 6. 1. In this table, the last two are the results of theoretical analysis by Yoshida, Kousaka and Okuyama, who proved the theoretical results by their own experiments.

Table 6. 1 Values of m of Eq. 6. 1.

Reporter	m	Type of apparatus
Jimbo and Fujita[37)]	0.8–2.0	suction of aggregates
Jimbo, Tsubaki and Nagahiro[39)]	1.0	sudden deceleration of aggregates
Watanabe[38)]	0.6	ejector
Yamamoto and Suganuma[35)]	0.6	capillary
Kousaka et al[36)]	0.5	capillary, orifice
Kousaka et al[36)]	<0.25	venturi

They analysed the mechanism of the failure by collision of agglomerates with obstacle and obtained the value of m as 0.5 theoretically.[36)] In this collision model, they assumed that the agglomerate was composed of two particles with different sizes and then calculated the stresses on the surface of both particles contacting each other. From their theoretical analysis, the stress breaking up the agglomerate was deduced, in Stokes' region, as follows

$$\sigma,\ \tau \propto \frac{u_r}{d_{ag}} \tag{6.2}$$

where u_r is the relative velocity and d_{ag} is the size of agglomerated particle.

The authors' intention was to deduce Eq. 6. 1 from Eq. 6. 2 theoretically, by analysing the break-up mechanism due to the relative velocity. About this breaking model, Bagster and Tomi had analysed the stress on the surface within the spherical agglomerate in uniform flow.[40)]

6. 2. 2. Theoretical analysis

To derive Eq. 6. 1 from Eq. 6. 2 theoretically, it is necessary to define the strength

of agglomerate and analyse the mechanism of break-up process.

As it has already been confirmed experimentally that coordination number of primary particles and cohesive force are distributed as indicated in Chapter 3, the local coagulate force in an agglomerate should be distributed. Therefore when the agglomerate includes some parts weaker than the failure force, it is assumed that break-up of the agglomerate is induced at these weak parts. In the case of break-up due to relative velocity, the strength of the agglomerate is controlled not by the average strength but by the number of weak coagulated parts. Then the strength, σ_{ag}, can be assumed to be inverse to the number of weaker parts, $n(\sigma_H<\sigma_{max},\ \tau_{max})$.

$$\sigma_{ag} \propto \frac{1}{n(\sigma_H<\sigma_{max},\ \tau_{max})} \tag{6.3}$$

If the distribution of local coagulation forces in any size of agglomerate is the same and all local coagulated parts weaker than the failure forces contribute to break up the agglomerate, $n(\sigma_H<\sigma_{max},\ \tau_{max})$ in Eq. 6. 3 is in proportion to the number of primany particle which composes the agglomerate and also the volume of the agglomerate.

$$n(\sigma_H<\sigma_{max},\ \tau_{max}) \propto n(d_{pl}) \propto {d_{ag}}^3 \tag{6.4}$$

On the contrary, if it is assumed that the agglomerate breaks up at some points on the surface or on cross-section in the agglomerate, then the number of weaker coagulated parts contributing to failure can be proportional to the square of the agglomerate diameter.

$$n(\sigma_H<\sigma_{max},\ \tau_{max}) \propto {d_{ag}}^2 \tag{6.5}$$

The relationship between the strength of agglomerate and the failure force is thus assumed as shown in Fig. 6. 1. As is obvious from Fig. 6. 1, all agglomerates larger than d_{agcrit} must be broken up, where d_{agcrit} is to satisfy the following equation.

$$\sigma_{max},\ \tau_{max} = \sigma_{ag} \tag{6.6}$$

When the strength of agglomerate is proportional to the cubic of size, the following equation is obtained by substituting Eqs. 6. 2 and 6. 4 into Eq. 6. 6.

$$d_{agcrit} \cdot {u_r}^{0.5} = K \tag{6.7}$$

When the strength is proportional to the square of the size, then the relation of

$$d_{agcrit} \cdot u_r = K \tag{6.8}$$

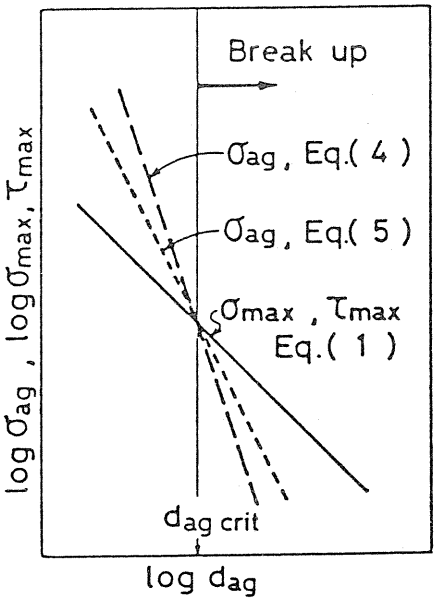

Fig. 6. 1. Relationship between the strength of aggregates and failure force.

is obtained from Eqs. 6. 2, 3, 5 and 6. The definition of particle size in these equations is different from that in Eq. 6. 1. But the value of index m is not so much affected by the definition of particle size after failure.

Therefore it can be said that the value of m in Eq. 6. 1 is between 0.5 and 1.0. The values of m in Table 6. 1 are well in this region, except a few.

6. 2. 3. Experimental methods by deceleration principle

To prove these relations described in the preceding two sections, the authors developed the experimental equipment for breaking up agglomerated particle in air flow by deceleration principle. As shown in Fig. 6. 2, the agglomerates were made by a

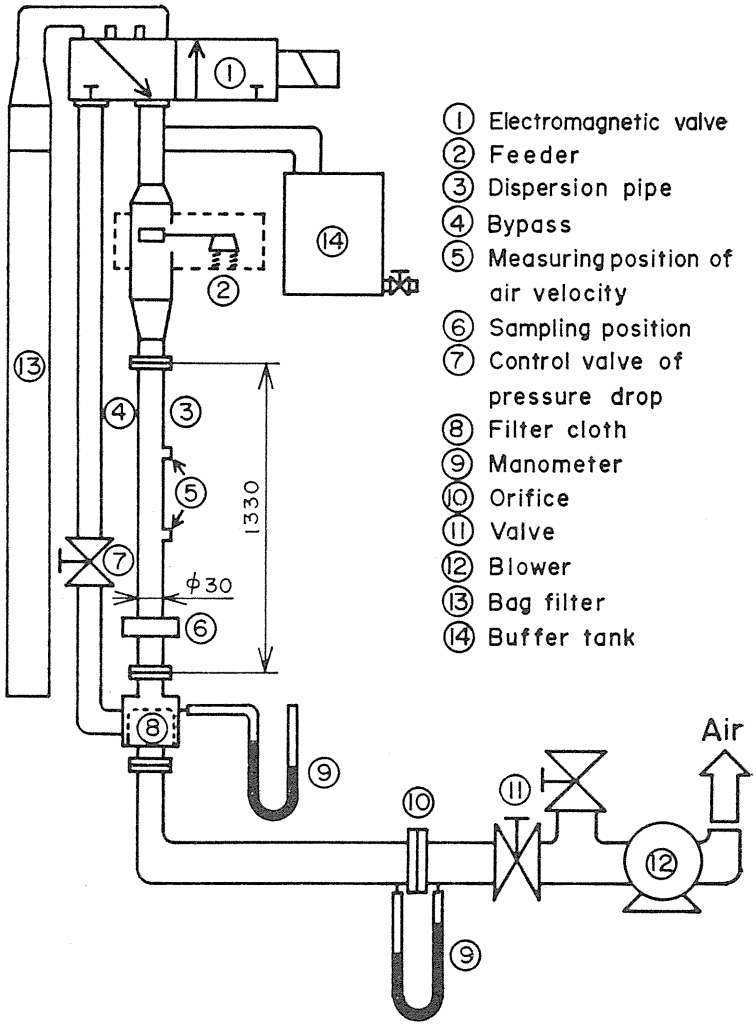

Fig. 6. 2. Experimental apparatus to break powder agglomerate in air flow.

feeding sieve, which made agglomeration and controlled the size of agglomerates. The agglomerates thus made were carried by air flow downward in a vertical tube steadily. The air flow stopped by shutting the electromagnetic valve on the top of the tube. A buffer tank was set to control the deceleration by filling it with the water. The air velocity was measured by a thermovelocimeter. From the air velocity measured like Fig. 6. 3, the velocity of particles, so that the difference of these two velocities was calculated.

Sampling was made by inserting a glass plate in the tube at the position close to the bottom. The size of agglomerate was measured by microscopic method, but here the largest diameter on one sampling slide glass was taken as the characteristic size of agglomerate before and after the failure, because the largest diameter showed the critically surviving agglomerate under the air flow conditions. Twenty slide glasses were taken per one experiment, and therefore from the diameters of twenty largest particles we obtained the size distribution of the largest diameters of maximum agglomerate as shown in Fig. 6. 4. 50% size of this distribution was used as characterized size of agglomerate.

The advantageous points of this method compared with acceleration method can be summarized as follows;

(i) There is no change of track of agglomerated particles in air flow, therefore it is relative easy to estimate maximum force exerted on particles by calculation.

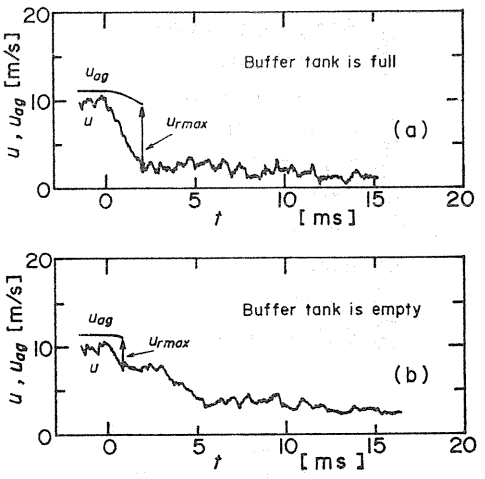

Fig. 6. 3. Air and aggregate velocity after the electro-magnetic valve is operated; Sample powder is limestone (d_{pl}=1.6 μm, ρ_{ag}=0.67 g/cm^3), mean air velocity U=10 m/s, opening of sieve=250 μm: a) deceleration α=376 m/s^2, diameter of feed aggregate d_{fmax50}=345 μm, b) α=288 m/s^2, d_{fmax50}=400 μm.

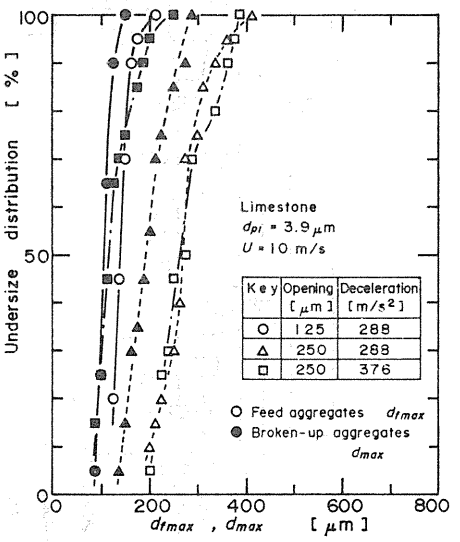

Fig. 6. 4. Undersize distribution of the maximum feed and broken-up aggregate on a sampling glass plate.

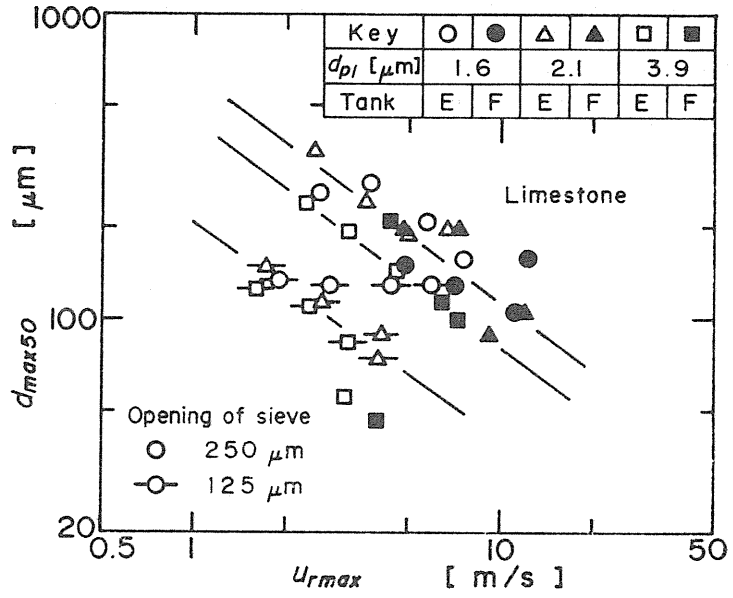

Fig. 6. 5. Relationship between diameter of broken-up aggregate and relative velocity (Limestone powder).

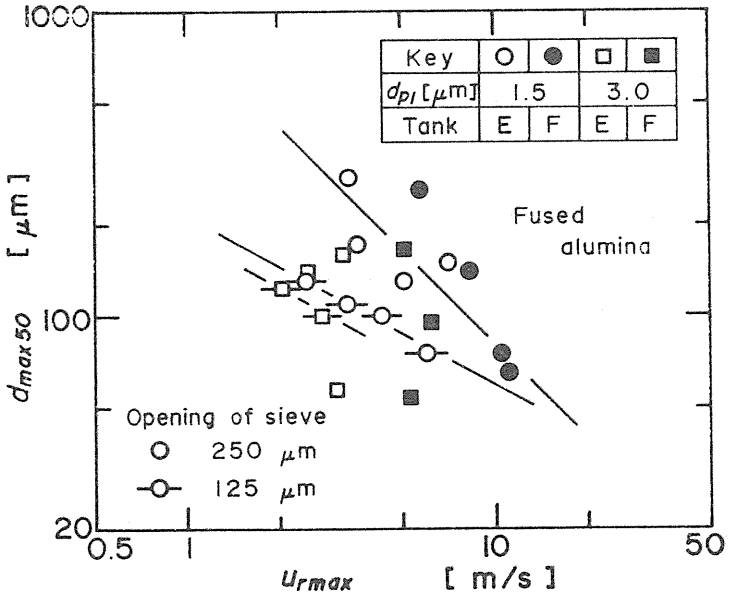

Fig. 6. 6. Relationship between diameter of broken-up aggregate and relative velocity (Fused alumina powder).

(ii) There is almost no possibility of the particles to collide each other or on the wall.
(iii) Sampling can be made in slowly sedimentating state, and then the breakage of agglomerates on sampling slide can be avoided.

Some experimental results expressed by the relation of u_{rmax} and d_{max50} are shown in Figs. 6. 5 and 6. 6. Considerable scattering of data obtained could not be avoided due to complexity of experimental procedure, but we can obtain from these figures the values of m as 0.5~0.7.

6. 3. Discussions

The relationship between the characterized velocity of air flow and the characterized size of agglomerated powder in equilibrium state, Eq. 6. 1, proposed by the author was reconfirmed theoretically and experimentally, and the theoretical value of exponent, m, was also derived as 0.5~1.0.

But the author's intention to find out the relation of these failure phenomena and the adhesive properties of powder has not yet been achieved. A qualitative tendency has been found that less adhesive powder makes smaller agglomerate in the same relative velocity. Comparing Figs. 6. 5 and 6. 6, we can find that the values of d_{max50} of fused alumina powder are relatively smaller than limestone powder, and the slope of lines is larger, that means that the agglomerates of fused alumina powder will be dispersed into primary particles in much smaller relative velocity.

But as you see in these figures, the sizes of primary particles are different, and the experimental results are very sensitive to experimental conditions. Therefore to find out the quantitatively characterized property, which controls the failure phenomenon of agglomerated powder in air flow, is still left for further investigation.

7. Measurements of mechanical powder properties at high temperature and their application

7. 1. Introduction

Many important chemical engineering processes which include powder materials are frequently used at high temperature, such as in fluidized bed reactor, rotary kiln and high temperature gas cleaning, and now their importance is growing up remarkably. But the behavior of powder materials at high temperature has not yet been investigated systematically.

As has been discussed in the preceding chapters, the measuring methods of mechanical powder properties have been developed rapidly and extensively, but those for high temperature measurement have hardly been investigated, except some important research works by the authors,[12)13)] and other groups.[41)42)43)44)]

In this chapter, the development of measuring methods of adhesion force and other characteristics of powder at high temperature which has been carried out in the authors' laboratory is presented with an example of their applications.

7. 2. Results of measurements of single particle

7. 2. 1. Measuring equipment used

For single particle measurement, the equipments of vibration and impaction separation methods, shown in Figs. 4. 1 and 2, were used by heating the cell parts of

these equipments with electric heaters. As they had been developed mainly for the applications at high temperature, there was no special problems about the equipments themselves and the procedure. But with these equipments, maximum temperature was about 500°C.

7. 2. 2. Results of measurement

The example of the measurement by vibration and impaction separation methods were shown in Figs. 4. 4 and 9. One additional example of almost the same result is shown in Fig. 7. 1. But in this figure, it is interesting that the 50 percent average value of adhesion force decreases against temperature rise. The same tendency was seen in Figs. 4. 4 and 9. There the adhesion force once dropped from 20°C to 110°C, and then again started to rise.

This tendency is more clearly shown in Fig. 7. 2, in which the results by several methods, including powder bed splitting method, are compared. The tendencies are all the same, namely according to the rise of temperature, the adhesion force once drops showing minimum value at about 100°C, and then starts to rise until nearly the melting point of the materials, where the maximum value appears. Other materials show almost the same tendency.

In Fig. 7. 3, the effect of particle size is shown in the case of coal powder. But here

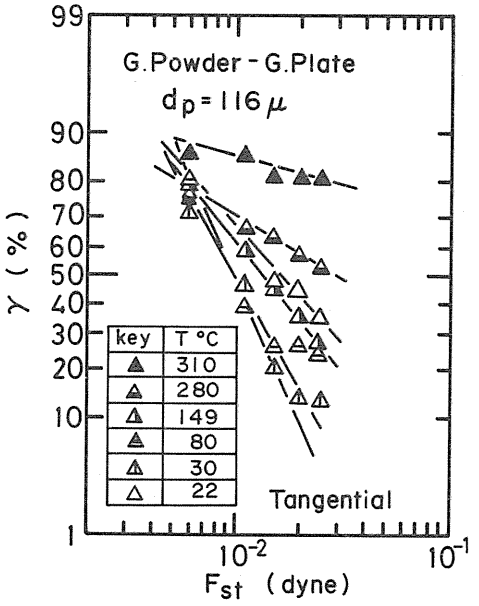

Fig. 7. 1. The effect of temperature on the separation force by vibration tangential separation method.

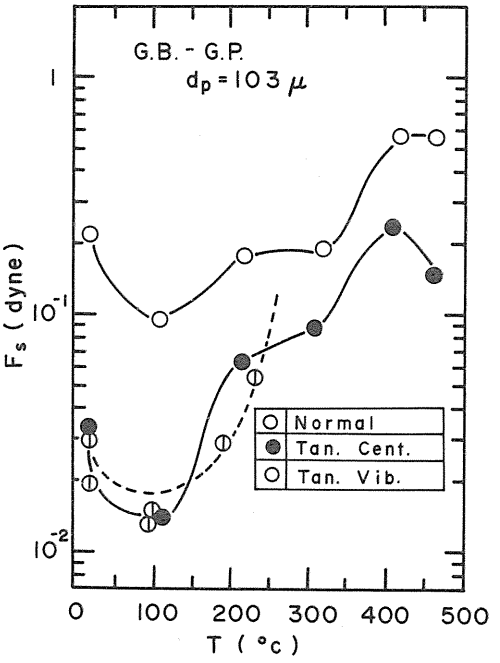

Fig. 7. 2. The effect of temperature on the average value of separation force of glass beads.

also the drop of adhesion force by rising temperature up to 200°C is shown. The effect of particle size is almost proportional to the diameter at room temperature as was found before, but at higher temperature the effect becomes larger, the reason of which has not yet been cleared.

7. 3. *Results of measurements of powder bed*

7. 3. 1. *Equipment and method used*[13]

Modified Warren Spring type split cell tensile tester was put in a furnace as shown in Fig. 7. 4. Compression of powder bed before or after heating is very essential factor to determine the tensile strength, and then the special compressing weight was put in this set-up as shown in the figure.

Two types of operation procedure were used, one was to fill the split cell with sample powder at an operating temperature and then to press it for compaction, which was denoted as "mode A", and another was to fill the cell and to press it first, and then to raise the temperature, which was denoted as "mode B".

The maximum temperature of this equipment was about 600°C, and the measurable range of porosity was limited.

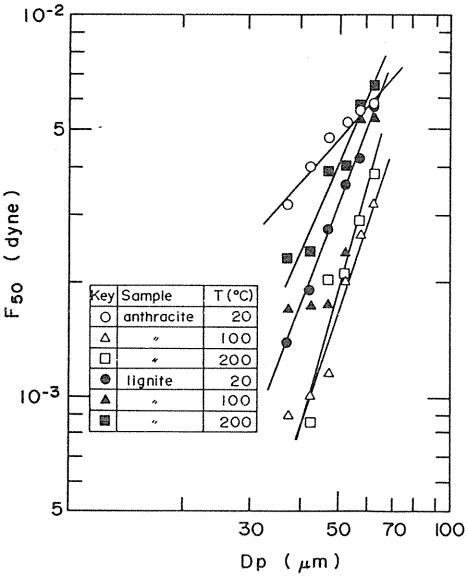

Fig. 7. 3. The effect of particle size on average adhesion force at different temperature.

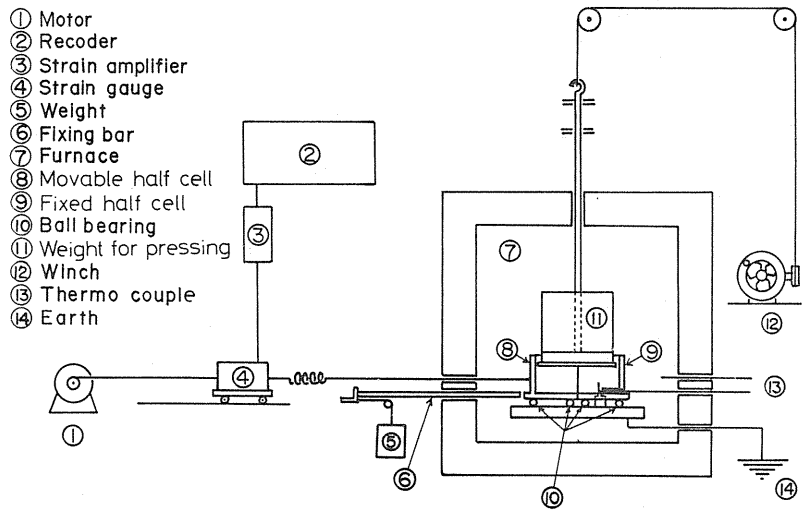

Fig. 7. 4. Split cell type powder bed tensile tester for high temperature measurement.

7. 3. 2. Results of measurement

(1) The effect of porosity on tensile strength of powder bed (Mode A procedure)

The relation between the tensile strength σ_z and the porosity ε of powder bed is represented on semi-logarithmic chart, as are shown in Figs. 7. 5 and 7. 6. It can be seen easily that in these figures there is no or only little change of strength σ_z, but very remarkable change of porosity according to the rise of temperature. In another word, the porosity of bed changes for keeping the strength constant. This phenomenon is more clearly shown in Fig. 7. 7, in which the tendency of the increase of the strength by increasing of the compression force, not by decreasing of the porosity, is indicated.

Therefore the measurement of the porosity of powder bed ε against temperature, as shown in Fig. 7. 8, can be another method to characterize the powder property against temperature. Afterward this principle has been developed by the authors successfully for higher temperature measurement, up to 1,000°C.[45]

The tendency of the same relation is obviously different in the case of fused alumina powder as are shown in Figs. 7. 9 and 10. There only a little change of porosity, and remarkably big change of tensile strength are seen. But when attention is paid to the effect of particle size, there again the horizontal change of porosity can be seen. This different tendency can be indicated in the relation between ε and T as is shown in Fig. 7. 11.

On the other hand, in the case of plastic powder shown in Fig. 7. 12, the relation between σ_z and ε is different. The change of the porosity and the strength occurs at the same time, and then all data come together onto a single line.

At this stage of investigation, it is not possible to explain these phenomena above mentioned, but it can be pointed out that there is a possibility to characterize the temperature dependent mechanical properties of powder bed by this relationship.

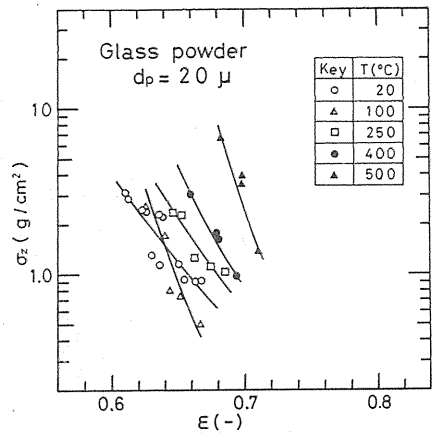

Fig. 7. 5. The effect of porosity, ε, on tensile strength of powder bed, σ_z (Glass powder).

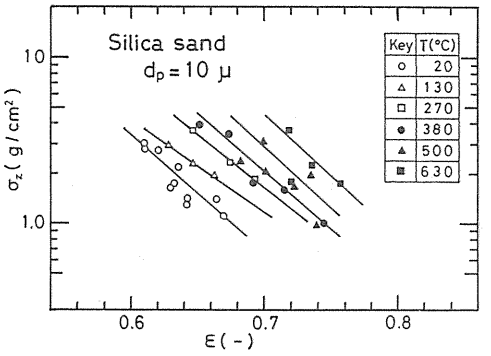

Fig. 7. 6. The effect of porosity, ε, on tensile strength of powder bed, σ_z (Silicate sand).

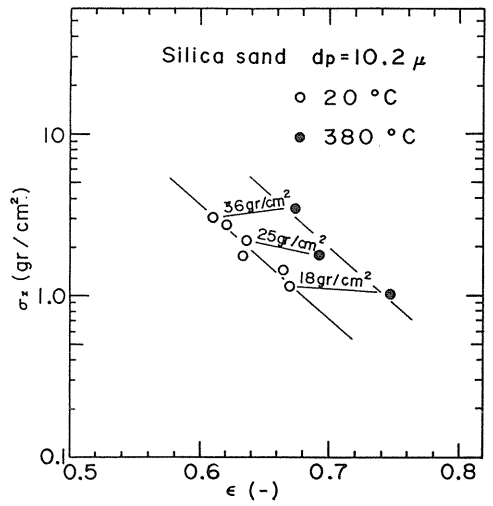

Fig. 7. 7. The effect of compression stress on the relation of $\varepsilon \sim \sigma_z$.

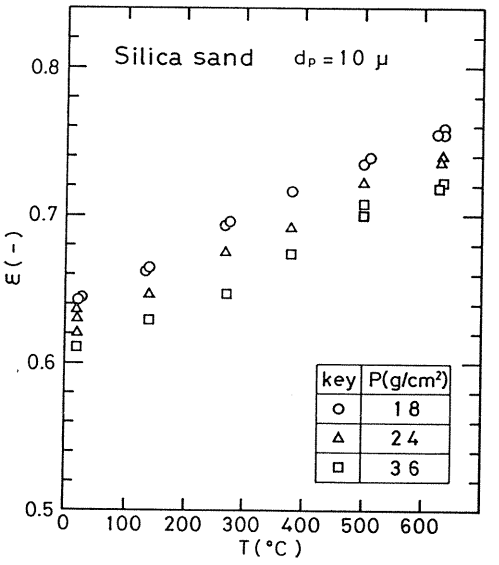

Fig. 7. 8. The change of porosity against temperature rise (Silicate sand powder).

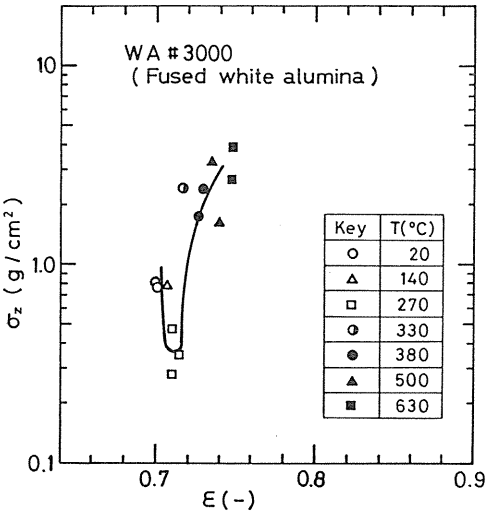

Fig. 7. 9. The effect of porosity, ε, on tensile strength of powder bed, σ_z (Fused alumina powder, coarse).

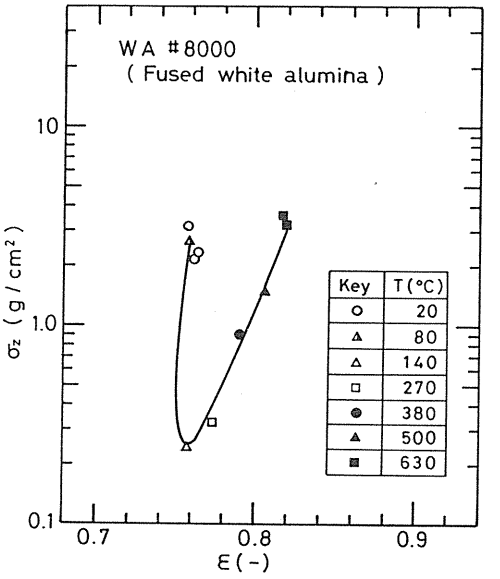

Fig. 7. 10. The effect of porosity, ε, on tensile strength of powder bed, σ_z (Fused alumina powder, fine).

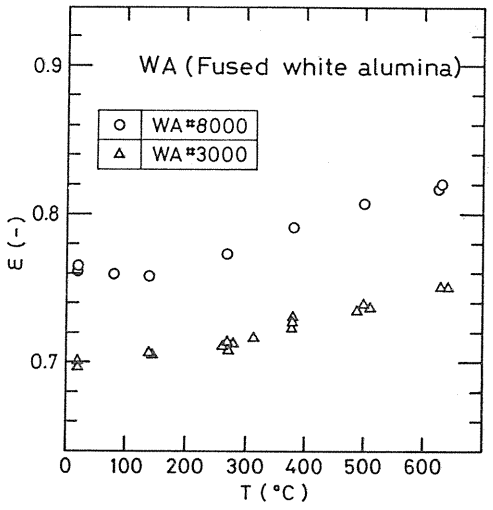

Fig. 7. 11. The change of porosity against temperature rise (Fused alumina powder).

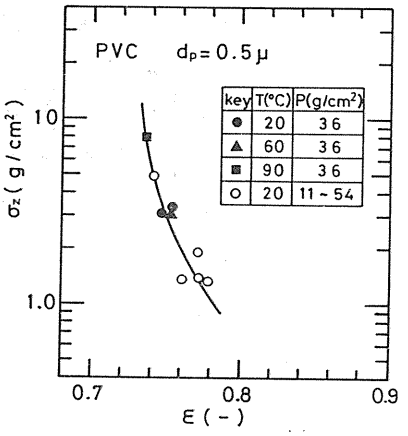

Fig. 7. 12. The effect of porosity, ε on tensile strength of powder bed σ_z (PVC powder).

(2) The change of strength of powder bed against temperature rise (Mode B procedure)

Fig. 7. 13 shows an example of the increase of tensile strength of silicate sand powder bed against temperature rise, keeping the porosity constant. (Mode B) In this figure, the strength of the bed at room temperature after cooling down a heated powder bed is also shown. This means that up to 600°C, there is almost no possibility of sintering. When that bed is disturbed, then the strength decreases to less than original perhaps because of the rearrangement of bed structure.

(3) Calculated value of single particle adhesion force from the tensile strength of powder bed

Figs. 7. 14 and 15 show the change of the adhesion force of single particle at high temperature calculated from the data of the tensile strength of powder bed using Rumpf's equation. Both figures show the effect of porosity and compression.

7. 4. Conclusions of Chapter 7

The measuring methods of the adhesion force of particles and the tensile strength of powder bed have been developed for high temperature measurement up to 400°C~600°C.

The adhesion force drops at about 100°C from room temperature, and then increases according to the rise of temperature in the range of lower than sintering point.

But the change of adhesiveness by heating causes different change of packing properties according to the materials themselves. This phenomenon must be investigated further,[45] but in this chapter only the possibility to make use of this change of packing property is pointed out.

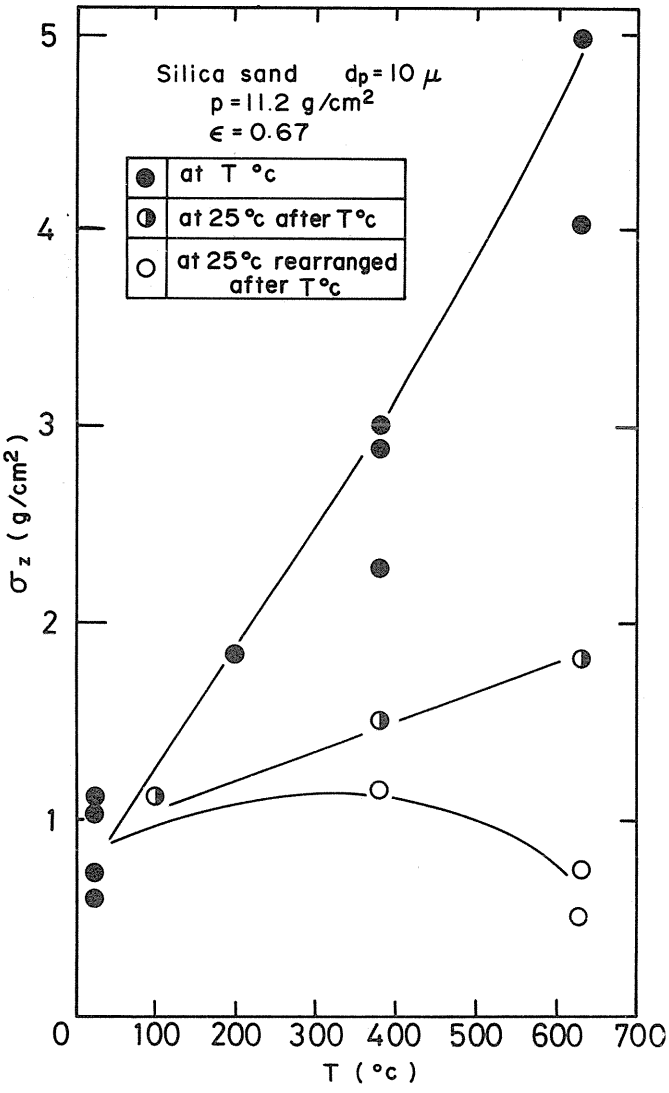

Fig. 7. 13. The effect of temperature on adhesion of powder bed.

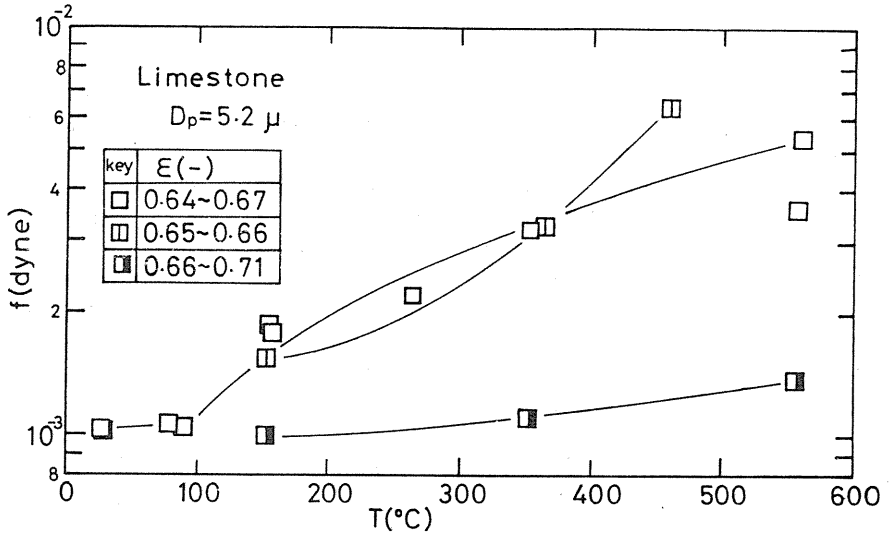

Fig. 7. 14. Change of adhesion force of single particle in powder bed with temperature (Limestone).

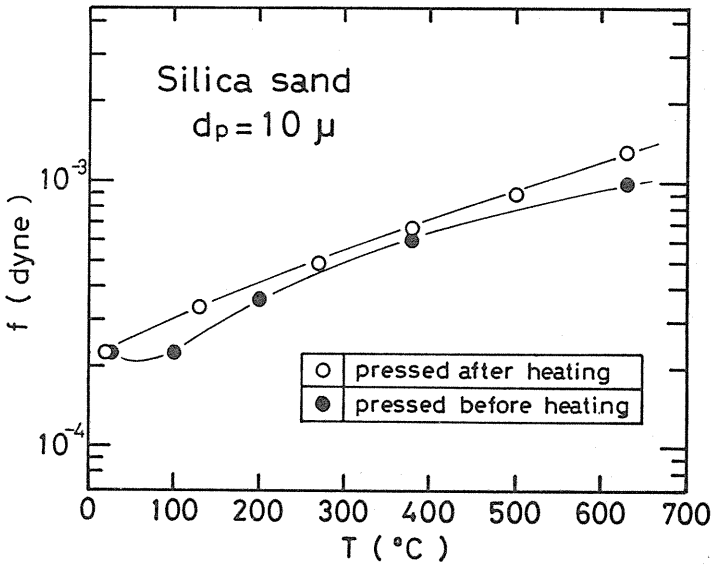

Fig. 7. 15. Change of adhesion force of single particle in powder bed with temperature (Silicate sand).

8. Mechanism of incipient fluidization in fluidized bed at elevated temperature

8. 1. Introduction

As one of the applications of the measured results of mechanical powder properties at high temperature, the mechanism of incipient fluidization was analysed. Many fluidized bed processes, such as chemical reactor, are operated at elevated temperature. Many workers have pointed out that the predicted value of incipient air velocity at elevated temperature showed remarkable discrepancy from the observed value, when only the increase of the viscosity of the air was taken into account.[46]

On this point, the authors have already pointed out that the change of adhesive force of particle and resulting change of the voidage of bed with temperature had to be taken into account.[47] Here the authors would like to propose new equation to predict the incipient fluidization velocity by applying the measured results of adhesion force at high temperature.

8. 2. Theoretical model proposed

The general concept of the model for predicting the voidage of a fluidized bed ε_{mf} is as follows: In the case of fluidized particles with sufficiently larger size than equilibrium diameter, each particle behaves as a single particle. But in the case of fluidized particles with high adhesiveness, the particles stick each other and behave as clusters consisting of two or more particles. When fluidized gas is reduced to the minimum fluidization velocity, these clusters settle down to form packed bed with relatively loose packing structure, because the clusters have an irregular shape. Accordingly, it can be assumed that ε_{mf} is expressed by a function of the shape factor of the cluster.

In addition to the above general concept, the following assumptions are also made ;[48]

(i) The shape factor of cluster, Φ, is given by

$$\Phi = \phi_p \cdot \phi_a \tag{8.1}$$

where ϕ_p is the shape factor of a single particle and ϕ_a is the shape factor of the cluster composed of spherical particles. And Φ can be written as follows;

$$\Phi = \frac{\phi_p}{n^{\frac{1}{3}}}\ 1+0.188\ \frac{n-1}{n} \tag{8.2}$$

where n denotes the number of particles in a cluster.

(ii) The number of single particle in a cluster can be derived from the balance of adhesion force, F_{ad}, and the separation force as follows

$$n = \frac{F_{ad}}{\frac{\pi}{6}\ k\rho_p {d_p}^3 g} \tag{8.3}$$

(iii) Adhesive force F_{ad} can be expressed as follows;

$$F_{ad} = cf(T){d_p}^2 \tag{8.4}$$

in which $f(T)$ denotes the ratio of the adhesive force at temperature T to that at room temperature.

(iv) The following equation analogous to Wen and Yu's equation[49] is assumed;

$$\frac{1}{\Phi^2}\,\frac{1-\varepsilon_{mf}}{\varepsilon_{mf}^3}=K \tag{8.5}$$

8. 3. Derivation of ε_{mf} and u_{mf} as the functions of particle size and temperature

Substitution of Eq. 8. 2 into Eq. 8. 5 gives the following equation;

$$\frac{\varepsilon_{mf}^3}{1-\varepsilon_{mf}}=\frac{1}{K\phi_p^2}\,\frac{n^{\frac{2}{3}}}{\left(1+0.188\dfrac{n-1}{n}\right)^2} \tag{8.6}$$

Since $0.188(n-1)/n \ll 1$,

$$\frac{1}{\left(1+0.188\dfrac{n-1}{n}\right)^2}\fallingdotseq 1-0.376\left(\frac{n-1}{n}\right)=0.624\left(1+\frac{0.603}{n}\right) \tag{8.7}$$

Using above approximation, Eq. 8. 6 can be expressed as follows

$$\frac{\varepsilon_{mf}^3}{1-\varepsilon_{mf}}=0.624\frac{n^{\frac{2}{3}}}{K\phi_p^2}\left(1+\frac{0.603}{n}\right) \tag{8.8}$$

Designating ε_{mf} at $n=1$ in Eq. 8. 8 by ε_{mfc}, this equation can be expressed as follows;

$$\frac{\varepsilon_{mfc}^3}{1-\varepsilon_{mfc}}=\frac{1}{K\phi_p^2} \tag{8.9}$$

Eliminating of $K\phi_p^2$ from Eqs. 8. 8 and 9 gives the final expression for the relation between ε_{mf} and n as follows;

$$\frac{\left(\dfrac{\varepsilon_{mf}^3}{1-\varepsilon_{mf}}\right)}{\left(\dfrac{\varepsilon_{mfc}^3}{1-\varepsilon_{mf}}\right)}=0.624n^{\frac{2}{3}}\left(1+\frac{0.603}{n}\right) \tag{8.10}$$

The relation between n, d_p and $f(T)$, can be obtained by substituting Eq. 8. 4 into Eq. 8. 3;

$$n=\frac{cf(T)}{\left(\dfrac{\pi}{6}\right)k\rho_p d_p g} \tag{8.11}$$

Designating the smallest size of particle which does not form a cluster at room temperature, i.e. the particle size at $f(T)=1$ and $n=1$, by d_{pc}, Eq. 8. 11 is expressed as follows;

$$n=f(T)\left(\frac{d_{pc}}{d_p}\right) \tag{8.12}$$

Substitution of Eq 8. 12 into Eq. 8. 10 finally leads to the following equations for $\varepsilon_{mf}^3/(1-\varepsilon_{mf})$.

$$\frac{\left(\frac{\varepsilon_{mf}^3}{1-\varepsilon_{mf}}\right)}{\left(\frac{\varepsilon_{mfc}^3}{1-\varepsilon_{mfc}}\right)}=0.624f(T)^{\frac{2}{3}}\left(\frac{d_{pc}}{d_p}\right)^{\frac{2}{3}}\left[1+\frac{0.603}{f(T)\ \frac{d_{pc}}{d_p}}\right] \tag{8.13}$$

for

$$f(T)\left(\frac{d_{pc}}{d_p}\right)\geqq 1 \tag{8.14}$$

while

$$\frac{\left(\frac{\varepsilon_{mf}^3}{1-\varepsilon_{mf}}\right)}{\left(\frac{\varepsilon_{mfc}^3}{1-\varepsilon_{mfc}}\right)}=1 \tag{8.15}$$

for

$$f(T)\left(\frac{d_{pc}}{d_p}\right)<1 \tag{8.16}$$

Using these equations and some approximations, the equation of calculating u_{mf} can be derived for the condition of $f(T)(d_{pc}/d_p)\geqq 1$;

$$u_{mf}=\frac{(\phi_p d_p)^2}{150}\ \frac{(\rho_p-\rho_f)g}{\mu f}\left(\frac{\varepsilon_{mfc}^3}{1-\varepsilon_{mfc}}\right)$$
$$\times k_1 f(T)^{\frac{2}{3}}\left(\frac{d_{pc}}{d_p}\right)^{\frac{2}{3}}\left[1+\frac{k_2}{f(T)\left(\frac{d_{pc}}{d_p}\right)}\right] \tag{8.17}$$

where

$$k_1=0.624,\quad k_2=0.603$$

8. 4. Experimental verification of proposed equation

To prove the theoretical analysis described in the preceding sections, experiments were carried out using a fluidized bed set-up shown in Fig. 8. 1. The bed column, made of stainless steel, was 60mm in diameter and 500mm in height. A stainless steel porous plate was used as a gas distributor.

The bed was heated to a scheduled temperature by electric heaters. After the temperature became constant, the air velocity was gradually reduced from that of fully fluidized state to that of static bed, and the relation between pressure drop and air velocity was measured to determine u_{mf}.

The bed voidage at minimum fluidization, ε_{mf}, was obtained from the height of the bed. The surface of the bed was detected by measuring the slight change of pressure along vertical axis with a pressure transducer. After u_{mf} and ε_{mf} were measured, the bed was returned to a state of incipient fluidization again in order to traverse a thermocouple in the axial direction of the bed. The difference of temperature between the top and the bottom of the bed was less than 4% of the operating temperature.

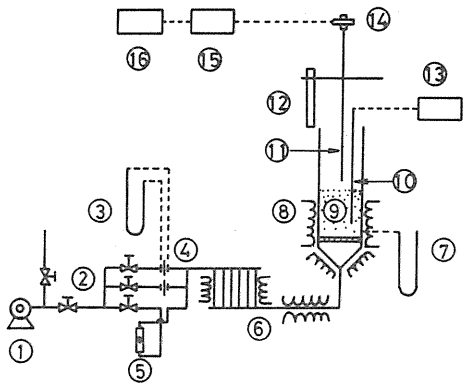

Fig. 8. 1. Schematic diagram of experimental apparatus.

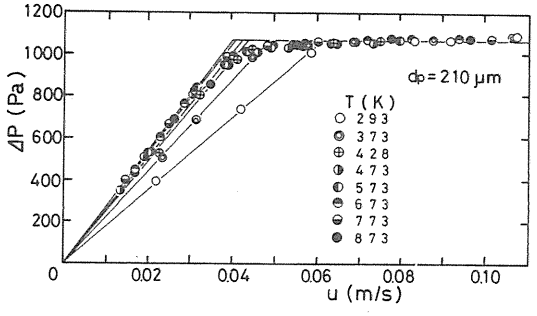

Fig. 8. 2. ΔP vs. u.

The change of the relation of Δp *and* u against temperature is shown in Fig. 8. 2, from which the change of u_{mf} against temperature can be obtained as Fig. 8. 3. The broken lines in this figure denote the calculated values obtained by assuming the bed voidage to be independent of temperature, and only the increase of the viscosity of the air was taken into account. The observed values of u_{mf} are much larger than the calculated values in high-temperature region. The values of ε_{mf} obtained are also shown in Fig. 8. 4. The general tendency is that ε_{mf} decreases with the increase of temperature below about 100°C, and then increases with the rise of temperature. This agrees with the

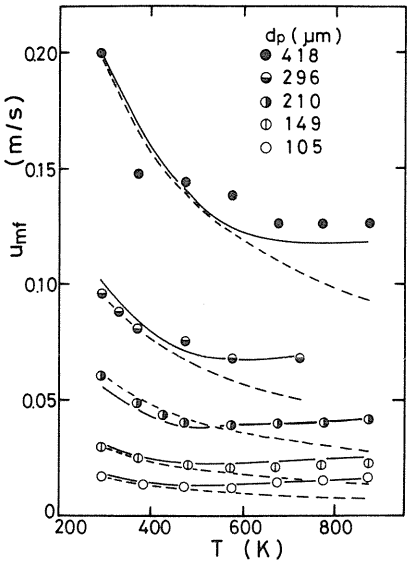

Fig. 8. 3. Variation of u_{mf} with temperature.

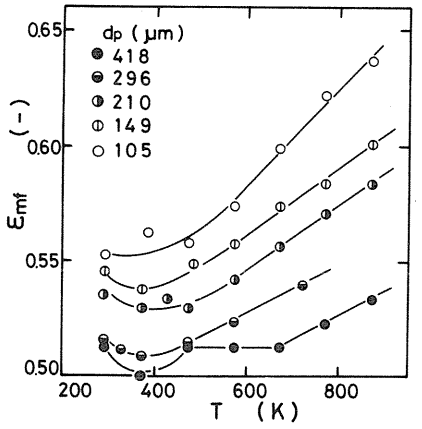

Fig. 8. 4. Variation of ε_{mf} with temperature.

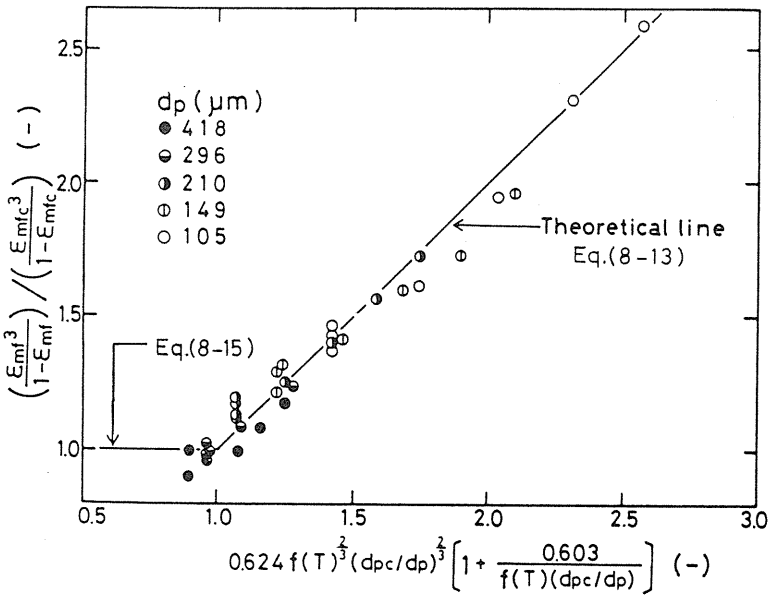

Fig. 8. 5. Comparison of observed ε_{mf} with calculated values.

results by two-dimensional bed,[47] and also seems to agree with the change of adhesion force shown in the preceding chapter.

Then the change of adhesion force with temperature obtained by tensile strength method shown in the preceding chapter was formulated as the function of $f(T)$ in Eqs. 8. 13 and 17. The critical values of ε_{mfc}, d_{pc} and ϕ_p were also obtained from this experiment as follows:

$$\varepsilon_{mf}=0.516,\ d_{pc}=260\mu m,\ \phi_p=0.633$$

The observed values of ε_{mf} are compared with those predicted by Eqs. 8. 13 and 15 in Fig. 8. 5. The theoretical equation well predicted the experimental value in fairly wide range.

The values of u_{mf} calculated by Eq. 8. 17 are also compared with the experimental values in Fig. 8. 6, which shows that the theoretical equation derived can predict the incipient fluidization velocity of high temperature fluidized bed up to 600°C well within ±10% error.

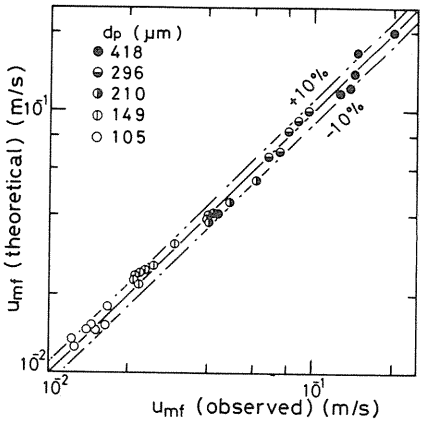

Fig. 8. 6. Comparison of observed u_{mf} with calculated values.

8. 5. *Conclusions of Chapter 8*

It was found that the change of adhesion force of powder particles affected to the incipient fluidization at elevated temperature. New theoretical equations, based on the cluster formation model of particles at high temperature, were derived, and they were proved experimentally taking into account of the change of mechanical powder property.

9. Measurement of time dependent mechanical powder properties

9. 1. *Introduction*

The mechanical powder properties which have hitherto been reported were all static and time independent. But in some cases, the authors have already found that the mechanical powder properties are time dependent. For instance, the effect of consolidation time of powder bed affected its strength. Famous Jenike shear cell adopted the measuring method with that effect. The tensile velocity to split powder bed affects the strength, and so on. In actual unit operations, we can find such time dependent properties, one example of which is the dislodgement of dust layer deposited on filter cloth. As the authors pointed out, this dislodgement occurs by the force considerably below the adhering strength of the dust layer to the filter cloth, after repeated exertion of impacting or vibratory force.[50]

Therefore there is a strong possibility that this time dependency of some properties might be the cause of big scattering of data and poor reproducibility of the measurement of powder particles.

Though this time dependency makes powder behavior more complicated, it is also very big source of informations about the packing structure, contacting relation and other interparticle relation of particles and powder bed. In a sense, "time dependent" relates "dynamic". Therefore it can be expected that the analysis of this time dependent properties could be the first step of the development of scientific measuring method of dynamic mechanical powder properties. Therefore to develop the measuring methods of time dependent mechanical powder properties is very important to improve the measurement itself and also to extend its functions.

9. 2. Experimental equipments used

To test the time dependent properties, basically three types of equipment were used. Tensile tester of hanging type for low frequency repeated stressing,[51)52)53)] a vibrator for high frequency stressing[54)55)] and a computer controlled press for compressing deformation and stress relaxation.[56)]

For creeping and low frequency fatigue phenomena, a hanging type split cell tester (Cohetester, Hosokawa Micron) was used (Fig. 9. 1 (1)), in which the spring with low elastic coefficient is put in between a movable cell and a pulley, as shown in this figure, for making loading velocity constant and creep test possible.

For high frequency fatigue test, a special cell shown in Fig. 9. 1 (2) was used by putting it on a vibrator. Sample powder bed was consolidated in a cylindrical cell, the upper part of which was removable. After powder bed was formed in the cell, the upper part of the cell was removed, and then the upper part of sample bed in it was exposed as shown in Fig. 9. 1 (2). The exposed part of powder bed was able to be separated by vibration force from another part of the bed fixed in lower part of the cylinder.

The maximum tensile stress exerted on the sectional surface in powder bed is described by the following equation,

$$\sigma_s = \frac{m_f(\alpha_o \omega^2 + g)}{A} \tag{9.1}$$

where m_f is the mass of separated powder bed, α_o is the amplitude of vibration, ω is angular frequency and A is the sectional area.

As the experimental method, sample powder was poured into the cell through shifting screen of 1 mm aperture, and consolidated for ten minutes, and then the upper surface of powder bed was formed accurately by scraping off the overpiled powder at the edge of the cell. Creep stress and vibration stress in the sample bed were exerted for about 10^4 sec. When the sample bed did not fail in this period, the strength of the bed under fatigue and creep histories was measured by increasing the loading force. The range of frequency was 5~300 Hz in dynamic repeated test. The preconsolidation stress was set and kept constant at 6.6 kPa for creep test, and in the region of 4.0~41.3 kPa for fatigue test. The conditions of temperature and humidity were kept constant at the range of 20°C±3°C and 50%±5%.

In the case of low frequency fatigue test, between 5 and 20 Hz, the experimental set up with a vibrator was connected to the movable split cell shown in Fig. 9. 1 (1).

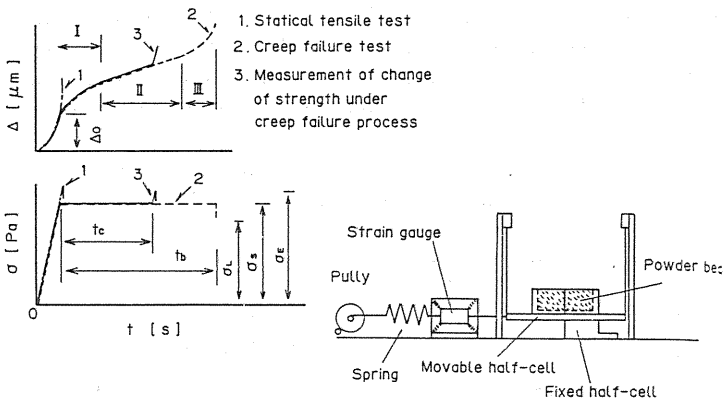

(1) For low frequency repeated load and creep test.

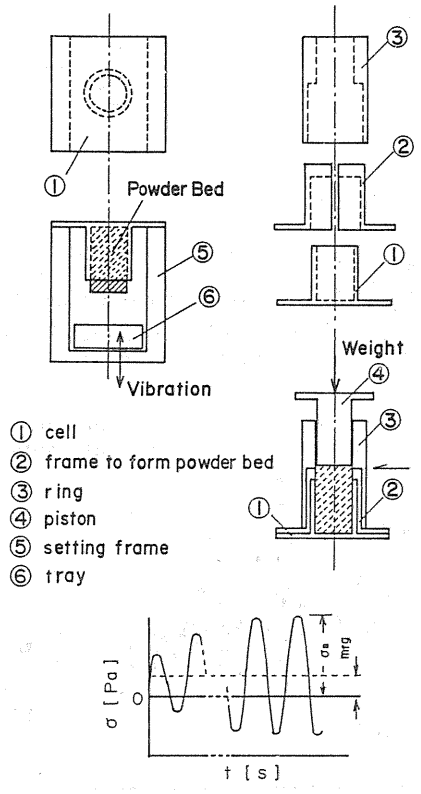

(2) For high frequency repeated stress.

Fig. 9. 1. Equipment used for time-dependent properties measurements.

9. 3. Relation between loading stress and fatigue life

The results of creep failure test are shown in Fig. 9. 2 as the relation between the creep tensile stress σ_s and the time required to make creep failure or creep life. Ordinate shows the ratio of creep stress to mean static tensile strength measured independently, so-called stress ratio. The black marks indicate unbroken data which did not fail in loading period t_c.

In Fig. 9. 2, the lower limits of stress, so-called endurance limit, below which there is no possibility of failing of powder bed, are also able to see. The creep life increases as

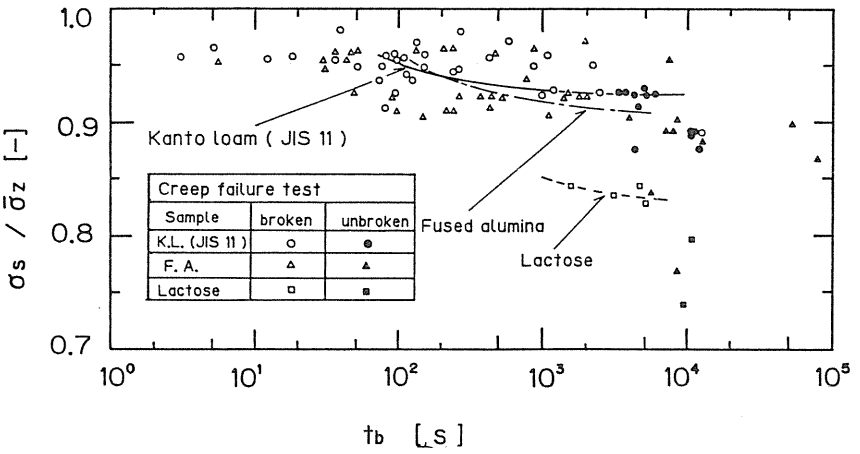

Fig. 9. 2. Loading stress-creep failure life relation.

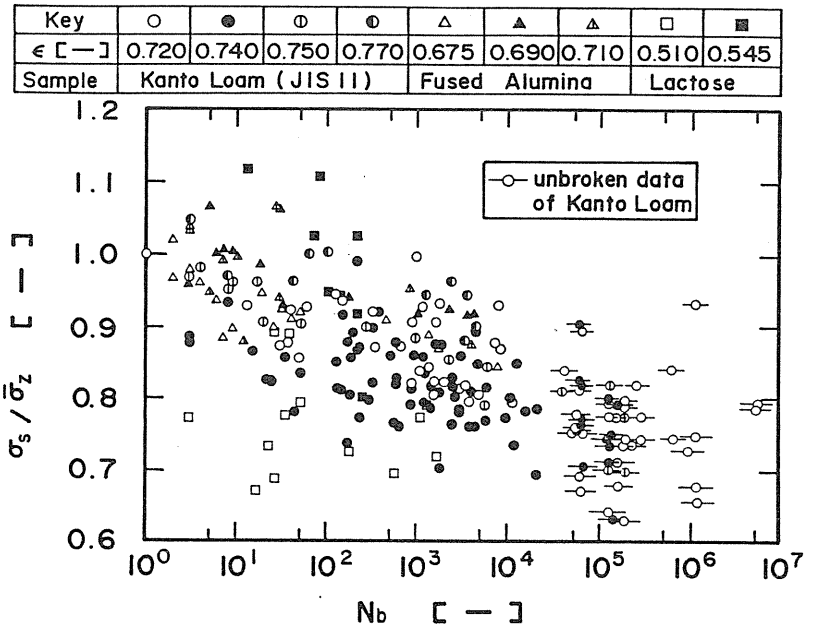

Fig. 9. 3. Relation between stress ratio and fatigue life (S-N relation).

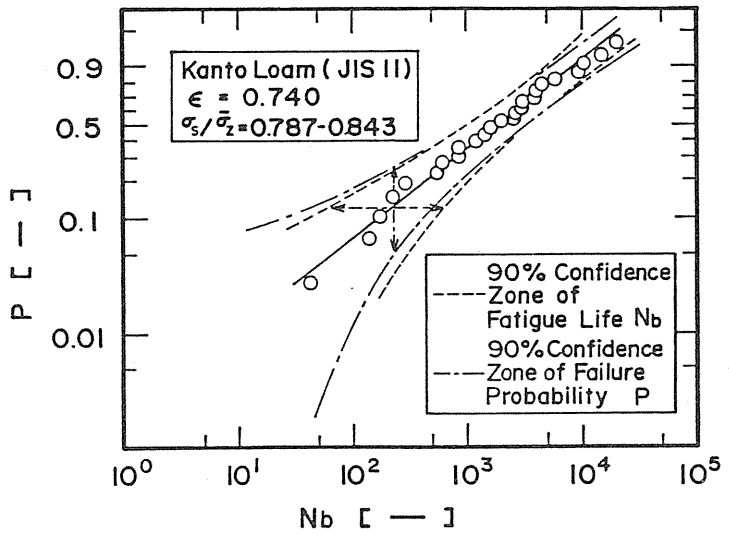

Fig. 9. 4. Fatigue life distribution of loam clay powder expressed by Weibull distribution.

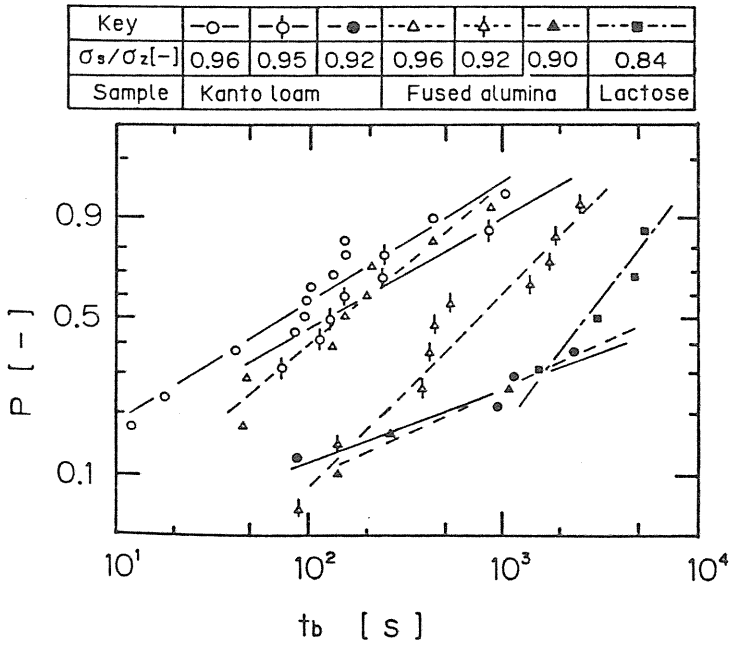

Fig. 9. 5. Creep fracture life distribution expressed by Weibull distribution.

the stress ratio decreases, and the lower limit of stress, where powder beds can not be failed in 10^4 sec, exists at 90% of mean tensile strength $\bar{\sigma}_z$ for Kanto loam clay (JIS Z8901, No. 11) and fused alumina powder, and at 80% of $\bar{\sigma}_z$ for lactose powder.

On the other hand, in the case of limestone powder, unbroken data exist even when the creep stress is slightly below $\bar{\sigma}_z$, and therefore creep failure phenomenon can not be found. From this result, it can be assumed that the endurance limit of two kinds of limestone powder is nearly equal to the mean value of static tensile strength, $\bar{\sigma}_z$. Accordingly the mechanical powder property can be characterized by the value of the endurance limit.

In the case of dynamic fatigue test, the same pattern was obtained, as is shown in Fig. 9. 3, in which the relation between the ratio of repeated maximum stress σ_s against the average of tensile strength $\bar{\sigma}_z$ and the number of repeated stress N_b are indicated. As are shown in Figs. 9. 2 and 3, the measured data of stress-life relation of powder bed scatter widely, therefore it is now necessary to develop more quantitative and analytical method about the distribution of the life.

9. 4. Statistical analysis of failure of powder bed[54]

To analyse the life distribution of powder bed, following methods are adopted. Firstly, the loading stress ratio ($\sigma_s/\bar{\sigma}_z$) is divided into some regions. And by using median rank, the failure probability gives each measured data in each region.

The distribution of failure life thus obtained can be expressed by the following Weibull's distribution function,

(a) creep failure test

$$P\ (t_b)=1-exp\{-(\frac{t_b}{t_p})^{m_c}\} \tag{9.2}$$

(b) fatigue failure test

$$P\ (N_b)=1-exp\{-(\frac{N_b}{N_p})^{m_r}\} \tag{9.3}$$

where t_p and N_p are the lives when the failure probability is 63.2%, or it can be said "characteristic life". m_c and m_r indicate the width of distribution, or it can be said "sharp parameter".

An example of the results of statistical analysis by using Weibull distribution obtained from fatigue failure test (Fig. 9. 3) is shown in Fig. 9. 4, and it indicates good linear relationship on Weibull distribution diagram. As the same results were obtained in creep failure test (Fig. 9. 5), it was confirmed that the distribution of failure life can be characterized by these two kinds of parameters in Weibull's equation. And the effect of $\sigma_s/\bar{\sigma}_z$ on the value of N is shown in Fig. 9. 6, where the sharp increase of $\bar{N}_p$ value according to the reduction of loading stress, σ_s, is seen and therefore we can reconfirm the existence of the endurance limit of fatigue failure phenomena. The smoothing curve in this figure corresponds to *S-N* curve popularly used in metallic materials tesing. The same results were also obtained in creep failure test.

The parameter of sharpness, m_c, which indicates the width of distribution obtained from Fig. 9. 5, is shown in Fig. 9. 7, for comparing the results of clay powder (Kanto

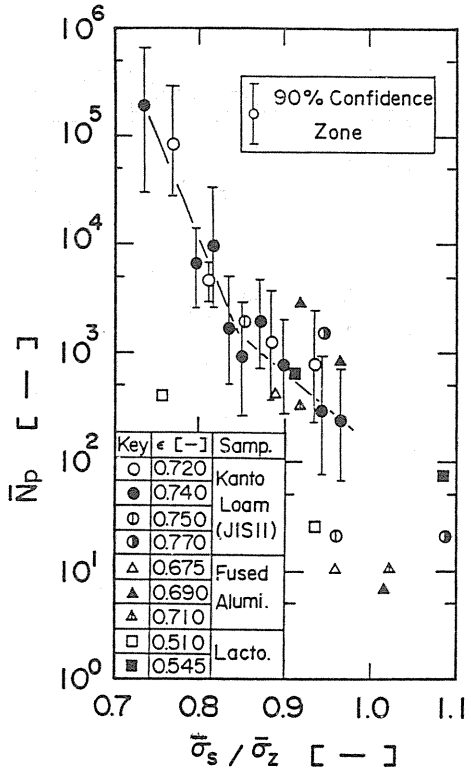

Fig. 9. 6. Estimation of the characteristic fatigue life in Weibull distribution.

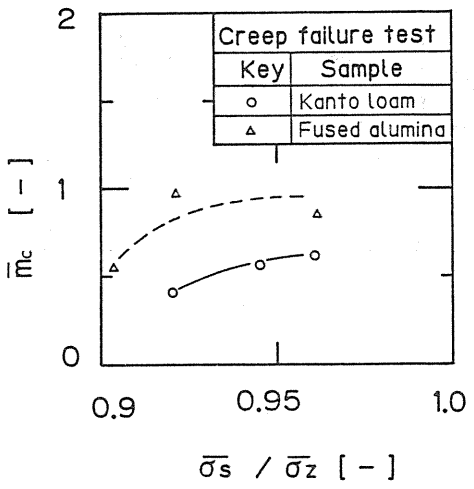

Fig. 9. 7. Shape parameter in Weibull distribution function and loading stress (Creep fracture test).

loam) and fused alumina powder. Though the endurance limits of these samples are almost the same (Fig. 9. 2), m_c are considerably different, namely the distribution of fused alumina powder is sharper than that of Kanto loam powder. On the contrary, the coefficients of variance, which indicates the scatter of static tensile strength, are 4.7% for fused alumina and 2.7% for Kanto loam. These results show an interesting contrast of the tendency between the distribution of failure life and the scatter of static tensile strength, and therefore they can be used for characterizing different aspects of mechanical properties of powder bed.

9. 5. Time dependent change of strength under creep history

To find out other characterization methods, the effect of creep history on the strength of powder bed was investigated experimentally using the hanging type tensile tester shown in Fig. 9. 1 (1). As is shown in Fig. 9. 8, the procedure was that after t_c sec loading of creep stress, σ_s, on powder bed, the strength under this creep history, σ_E, was measured by increasing the stress until failure occurred, to find the change of the strength by creeping.

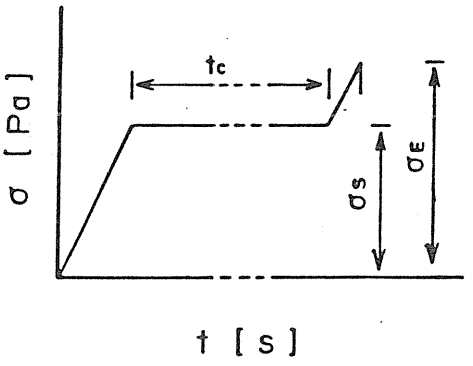

Fig. 9. 8. Schema of change of loading test during the test measuring strength of powder beds after creeping.

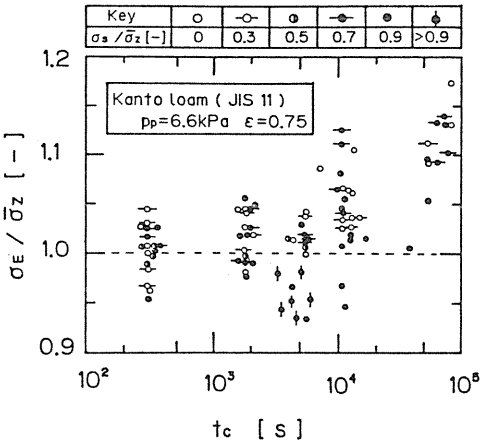

Fig. 9. 9. Change of the strength of powder bed by creeping history (Kanto loam clay).

An example of the measured results of Kanto loam clay powder is shown in Fig. 9. 9. This figure indicates the relation between the creeping period t_c and the strength σ_E, which is normalized by mean static strength $\bar{\sigma}_z$. This figure shows the apparent effect of creeping time on the strength, though the data are largely scattered. But it is clear that in the creeping condition of $\sigma_s/\bar{\sigma}_z \leq 0.7$, the strength of powder beds continues to increase after 10^5 sec loading. In such a case, it can be assumed that these beds would not fail.

Fig. 9. 10 shows the same result of limestone powder, which confirms the existence of strength increasing phenomenon very clearly. The same were found in other sample materials. And then comparing all of the results of several materials, the relations

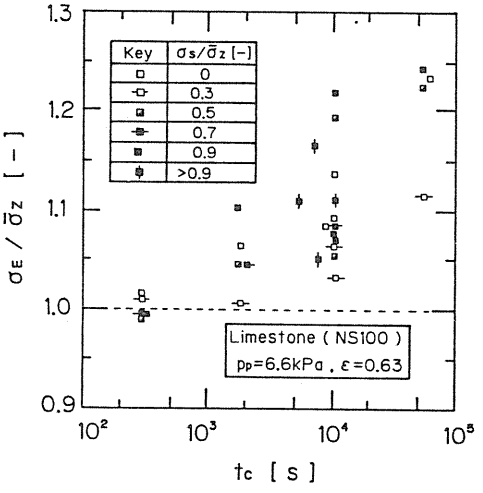

Fig. 9. 10. Change of the strength of powder bed by creeping history.

between the strength of powder bed after creeping of $t_c \doteqdot 10^4$ sec and the creeping stress ratio of several materials are shown in Fig. 9. 11. This figure also shows that in the region of $\sigma_s/\bar{\sigma}_z \geq 0.8$, where the endurance limit exists in all sample tests as shown in Fig. 9. 2, the strength after creeping tends to be smaller than that in the region of $\sigma_s/\bar{\sigma}_z < 0.8$. Comparing this tendency of each sample in this region, it was found that in the case of Kanto loam clay, fused alumina powder and lactose powder, of which the existence of creeping failure phenomenon was confirmed in some stress range, the value of σ_E was approximately equal to its static tensile strength, σ_E, and no increase of strength was observed. On the other hand, in the case of two kinds of limestone powder, of which creep failure could hardly be found, the value of σ_E was bigger than $\bar{\sigma}_z$ in almost all region.

In the region below endurance limit ($\sigma_s/\sigma_z < 0.8$), it was confirmed that the increasing phenomenon of the strength existed even at $\sigma_s = 0$, and is also independent of the value of creeping stress, σ_s. Based on these observations, it can be assumed that these phenomena do not depend only on the tensile stress, but mainly take place in connection with the consolidation and relaxing precedure of powder bed.

Summarizing these results described above, the schematical and diagramatical representation can be shown as Fig. 9. 12. In the case of Kanto loam clay powder expressed with hard line in Fig. 9. 12, the strength of powder bed is almost constant at the value of

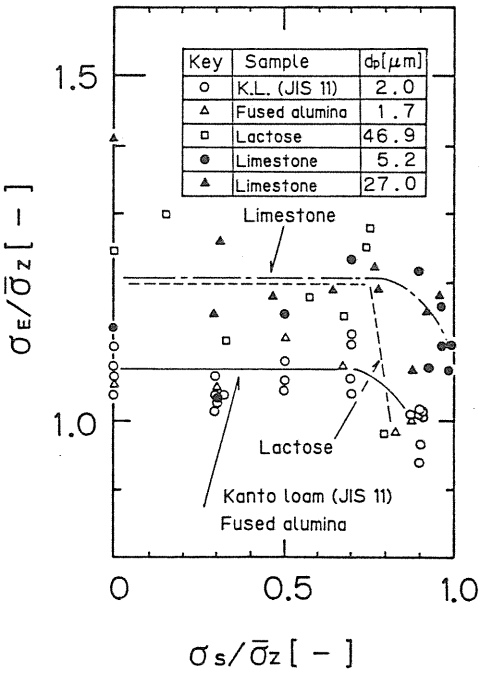

Fig. 9. 11. Relation between strength after creeping and creeping stress.

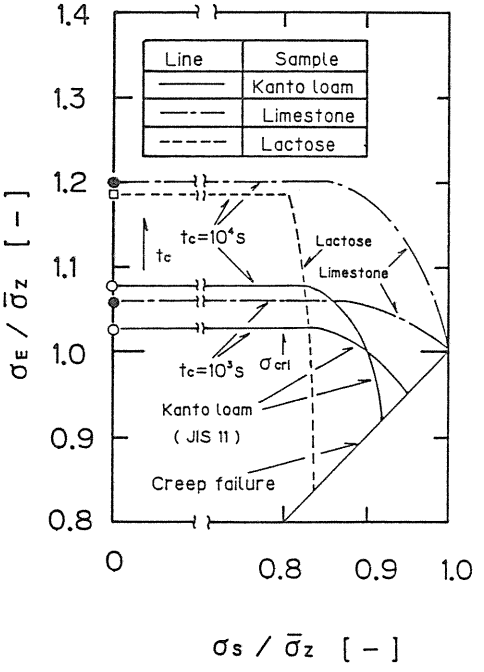

Fig. 9. 12. Characterization of change of strength after loading creeping history.

the strength at $\sigma_s=0$ below endurance limit, $\sigma_s<\sigma_{lim}$. The reducing phenomenon of the strength by creeping tensile stress occurs at some critical stress, σ_{cri}, and proceeds even beyond the point where σ_E is equal to $\bar{\sigma}_z$.

On the other hand, in the case of lactose powder indicated with broken line in the same figure, the increasing ratio of strength in the region $\sigma_s/\sigma_z<0.8$ is larger than Kanto loam powder, but the reducing effect appears at higher creeping stress ratio. In the case of limestone powder, as the increasing phenomenon exceeds the reducing effect in almost all region of the creeping stress ratio, the existence of the creeping stress attaining $\sigma_E=\bar{\sigma}_z$ after creeping of 10^4 sec can not be confirmed.

Based on the results above described, it can be concluded that the endurance limit is determined by two factors, one is increasing strength phenomenon and another is reducing effect by creeping tensile stress. The difference of the relations between these two factors determines the characteristics of time dependent failure phenomenon, and therefore they can be used as a new characterizing method of mechanical powder properties. The graphical representation shown schematically in Fig. 9. 12 is proposed as a new mapping method of mechanical powder properties, especially those related to time dependent properties.

9. 6. Conclusions of Chapter 9

(1) The existence of endurance limit, which is the lower limit of stress where powder bed fails, is confirmed with several kinds of materials.
(2) The endurance limit is determined by two factors of increasing phenomenon and reducing effect by creeping tensile stress. And the relation of these two factors is dependent upon materials themselves.
(3) The distribution of failure life can be expressed by Weibull distribution function, and the value of a Weibull parameter, which expresses the width of distribution, does not correspond to the scatter of static tensile strength.

Based on those results (1), (2) and (3), it can be concluded that the distribution of failure life, endurance limit strength, increasing phenomenon and strength reducing effect of tensile stress all have possibilities to characterize mechanical powder properties, which can not be characterized by the other static failure methods which have widely been used. New graphical representation method to characterize time dependent properties of powder bed is also proposed.

10. Conclusions

To extend the range of measuring conditions and to improve the reproducibility of the measuring methods of mechanical powder properties, several kinds of new measuring methods of mechanical powder properties, mainly about that of adhesive, have been developed and investigated by the authors. The methods cover from the single particle measurement to the measurements of tensile strength of powder bed, in which those with time dependent properties are included. The essential factors which control the measured results are analytically investigated.

Very large scattering of data obtained by various different methods was specifically investigated and the followings are pointed out as the main reasons for big difference of adhesive properties of powder materials with different method.
(1) The adhesion force of powder particles itself has a very wide distribution.

(2) The shape of a particle is very essential, especially related to contact relation of particles.
(3) The direction of separation force is very deterministic together with the contacting relation of particles. The equation to predict this effect is proposed.
(4) The stress exerted at the contact point of particles is one of the most controlling factors. The formation methods of powder bed and their conditions are very deterministic. To formulate this effect, modified Rumpf's equation is proposed.
(5) Besides the effect of humidity, the effect of temperature is another important factor. Especially the sharp drop of adhesiveness at about 100°C might be very influential to the measured results.
(6) Several kinds of time dependent properties are found and pointed out. They may be the other influential factors to determine the strength and other mechanical properties of powder bed.

Acknowledgement

The authors wish to thank Mr. S. Hatano for his excellent works on design and operation of new instruments developed in our laboratory. Thanks must be extended to Mr. S. Asakawa and Dr. M. Naito for their contributions to this research project. The helps by their ex-students both in master course and bachelor course, who have been involved in this project, are also very much appreciated.

The authors also acknowledge the financial supports to this research project by
Ministry of Education, Science and Culture
(Grant-in Aid for Scientific Research, No. 443624 (1979, 1980)
Asahiglass Foundation for Industrial Technology
(1978, 1979)
Fuji Xerox Co., Ltd.
Mita Industrial Co., Ltd.
and
Hosokawa Micromeritics Lab., Ltd.

Literature cited

1) Jordan, D. W.: *Brit. J. Appl. Phys.*, **3** s 194 (1954)
2) Larsen, R. L.: *Am. Ind. Hygiene Assoc. J.*, **19** 265 (1958)
3) Kordecki, M. C. and C. Orr, Jr.: *Arch. of Environmental Health*, **1** 1 (1960)
4) Krupp, H.: *Advances in Colloid and Interface Science*, **1** (No. 2) 113 (1967)
5) Zimon, A. D.: *Adhesion of Dust and Powder* (Trans. ed. M. Corn), Plenum Press (1969)
6) Ashton, M. D., R. Farley and F. H. H. Valentin: J. Sci. Instrum., **41** 673 (1964)
7) Jenike, A. W.: *Third Congress of European Federation of Chemical Engineering*, London, D.26 (1962)
8) Asakawa, S. and G. Jimbo: *Zairyo (J. Soc. of Materials Sci., Japan)*, **16** (164) 358–363 (1967)
9) Jimbo, G., S. Asakawa and N. Soga: *ibid*, **17** (177) 540–544 (1968)
10) Jimbo, G.: *ibid.* **16** (164) 291–297 (1967)
11) Jimbo, G.: *J. Soc. Powder Tech., Feb. 1966, Special issue on Adhesion and Agglomeration*, p. 27

12) Jimbo, G. and R. Yamazaki: *Reports of the Asahi Glass Foundation for Industrial Technology*, Vol. 38 p. 123–134 (1981)
Jimbo, G. and R. Yamazaki: *KONA-Powder Science and Technology in Japan*, No. 1, p. 40–47 (1983)
13) Jimbo, G., R. Yamazaki and Jun-ichiro Tsubaki, *Proceedings of 4th International Symposium on Agglomeration*, June 1985, Toronto, p. 697–702
14) Polke, R.: *Chemie-Ing.-Technik,* **40** 1057 (1968)
15) Jimbo, G. and S. Hatano: *Particle Characterization,* **1** 133–136 (1984)
16) Kaya, N., K. Fujii and T. Yokoyama: *Funsai (The Micromeritics),* **22** 32–38 (1977)
17) Jimbo, G. and R. Yamazaki: *European Symposium Particle Technology*, 1980, Amsterdam, B 1064
18) Otsuka, A. and K. Danjyo: *J. Soc. Powder Technology, Japan,* **18** 591 (1981)
19) Tsubaki, J., K. Kato and G. Jimbo: *ibid,* **18** (12) 873–879 (1981)
20) Naito, M., N. Kato, G. Jimbo and T. Yokoyama: *ibid,* **23** (7) 500–506 (1986)
21) Naito, M., S. Usuda, N. Kato, J. Tsubaki and G. Jimbo: *ibid,* **24** (7) 455–461 (1987)
22) Naito, M., S. Usuda, J. Tsubaki and G. Jimbo: *ibid,* **24** (8) 527–534 (1987)
23) Tsubaki, J. and G. Jimbo: *Powder Technology,* **37** 219–227 (1984)
24) Rumpf, H.: *Chemie-Ing.-Technik,* **42** 538 (1970)
25) Nagao, T.: *Kikaigakkai-Ronbunshu,* **43** 4038 (1977), *Bulletin of the JSME,* **21** 1077 (1978)
26) Molerus, O.: *Powder Technology,* **12** 259 (1975)
27) Kanatani, K.: *J. Soc. Powder Tech.,* **17** 504 (1980)
28) Tsubaki, J.: *ibid,* **21** (1) 30–39 (1984)
29) Tsubaki, J.: *KONA-Powder Technology in Japan*, No. 2 (1984), p. 78–86
30) Tsubaki, J.: *J. Soc. Powder Techn.,* **22** (9) 645–649 (1985)
31) Jimbo, G.: Kuki-Seijyo, **3** (1) 34–39 (1965)
32) Suh, T. S., T. Shibata, J. Tsubaki and G. Jimbo: *J. Soc. Powder Techn.,* **21** (1) 11–17 (1984)
33) Borho, K.: Staub, **33** 317 (1973)
34) Zahradnicek, A. and F. Löffler: *Intern. Chem. Eng.,* **19** (1) 40–45 (1979)
35) Yamamoto, H., A. Suganuma and D. Kunii: *Kagakukogaku-Ronbunshu,* **3** 12–18 (1977)
36) Kousaka, Y., K. Okuyama, S. Shimizu and T. Yoshida: *J. Chem. Eng., Japan,* **12** 152 (1979)
37) Jimbo, G. and S. Fujita: *Proc. Powtech, '71*, p. 155 (1971)
38) Watanabe, H., T. Matsuno and Y. Nakata: *40th Annual Meeting of Soc. Chem. Eng., J.*, 1978 Nagoya, Preprint p. 296
39) Tsubaki, J., K. Kato, Y. Nagahiro and G. Jimbo: *Kagakukogaku-Ronbunshu,* **9** (2) 189–194 (1983)
40) Bagster, D. F. and D. Tomi: *Chem. Eng. Sci.,* **29** 1773 (1974), **30** 269 (1975)
41) Jayasinghe, S. S.: *J. Inst. Fuel.,* Feb. 1970, p. 51
42) Pilpel, N. and J. R. Britten: *Powder Technology,* **22** 33–44 (1979)
43) Danjyo, K., K. Iida and A. Otsuka: *J. Soc. Powder Techn., Japan,* **19** (9) 530–537 (1982)
44) Oshima, T., M. Hirota and M. Suzuki: *J. Soc. Powder Techn., Japan,* **20** 357 (1983)
45) Jimbo, G.: *Annual IFPRI Report, ARR-11-8* (1988, May)
46) Yamazaki, R. and G. Jimbo: *J. Soc. Powder Techn.,* **20** (6) 357–380 (1983)
47) Hong, G. H., R. Yamazaki and G. Jimbo: *Kagaku Kogaku Ronbunshu,* **7** (2) 109–114 (1981)
48) Yamazaki, R., N. Ueda and G. Jimbo: *J. Chem. Eng., Japan,* **19** (4) 251–257 (1986)
49) Wen, C. Y. and Y. H. Yu: *AIChE. J.,* **12** 610 (1966)
50) Tsubaki, J., M. Naito, H. Tagami, F. Kousaka and G. Jimbo: *Kagaku Kogaku Ronbunshu,* **8** 481 (1982)
51) Tsubaki, J., K. Kato, T. Takeyama and G. Jimbo: *ibid,* **10** (3) 402–404 (1984)
52) Kamiya, H., J. Tsubaki and G. Jimbo: *ibid,* **11** (2) 210–215 (1985)
53) Kamiya, H., J. Tsubaki and G. Jimbo: *ibid,* **11** (3) 356–358 (1985)
54) Kamiya, H., J. Tsubaki and G. Jimbo: *ibid,* **11** (2) 186–192 (1985)
55) Kamiya, H., S. Furukawa, J. Tsubaki and G. Jimbo: J. Soc. Powder Techn., **22** (9) 618–625 (1985)
56) Kamiya, H.: PhD-Dissertation, Nagoya University, p. 66 (1986)

Nomenclature

A:	Area of fracturing surface	[mm^2]
a:	area of contacting plane	[mm^2]
b:	constant in Eq. 5. 4	[−]
c:	constant in Eq. 5. 6	[−]
d_{ag}:	diameter of agglomerates	[mm, μm]
d_p:	particle diameter	[mm, μm]
E:	Young's modulus	[Kg/mm^2, Pa]
F:	force (usually separation force)	[N]
F_{ad}:	adhesion force of a particle at a contact point	[dyne, N]
f_{ad}:	adhesion force per unit area	[$\frac{dyne}{cm^2}$, $\frac{N}{cm^2}$]
F_s:	separation force (suffix n: normal, t: tangential)	[dyne, N]
g:	gravitational acceleration	[m/s^2]
k:	constant	[−]
k_1:	experimental constant of Eq. 5. 4	[kPa]
	experimental constant of Eq. 8. 17	[−]
k_2:	experimental constant of Eq. 5. 5	[kPa^{1-m}]
	experimental constant of Eq. 8. 17	[−]
k_3:	experimental constant of Eq. 5. 6	[kPa]
m:	mass of powder	[g]
	experimental constant of Eq. 5. 5	[−]
m_c:	parameter of sharpness in Weibull's formula in Eq. 9. 2	[−]
m_f:	mass of separated powder bed	[g]
m_r:	parameter of sharpness in Weibull's formula in Eq. 9. 3	[−]
N_b:	number of repeated stress	[−]
n:	number	[−]
P:	compression force	[dyne, N]
p:	compression stress	[N/cm^2, kPa]
T:	tension	[N]
t:	time	[s]
t_c:	loading period	[s]
u:	air velocity	[cm/s, mm/s]
u_{mf}:	minimum fluidization velocity	[cm/s]
u_r:	relative velocity of a particle and air	[cm/s]
α:	amplitude of vibration	[mm]
	coefficient about angle relation of contact	[−]
β:	coefficient about the effect of packing structure	[−]
γ:	residual percentage	[%]
ε:	porosity of powder bed	[−]
ε_{mf}:	porosity at minimum fluidization velocity	[−]
μ_f:	viscosity of fluid	[Pa·s]
ν:	Poisson's ratio	[−]
ρ:	density (suffix s: solid, f: fluid)	[g/cm^3]
σ:	standard deviation	[−]
	strength of powder bed in general	[N/cm^2]

σ_E :	static strength after creeping	[N/cm^2]
σ_s :	creep tensile stress	[N/cm^2]
σ_z :	tensile strength of powder bed	[N/cm^2, kPa]
τ :	shear stress	[N/cm^2]
ϕ :	angle of slope	[°]
Φ :	shape factor (suffix p : particle, a : cluster)	[−]
ω :	angular velocity	[rad/s]